Earth, Planets and Space

FULL PAPER Open Access

International geomagnetic reference field: the fourteenth generation

C. D. Beggan[1*], C. Kloss[2], P. Amblard[3], T. Amezza[4], H. Amit[5], J. Aubert[6], J. Baerenzung[7], J. Bregnhøj Lauridsen[2], W. Brown[1], S. Califf[8,9], S. A. Campuzano[10,11], L. Chauvet[6], A. Chulliat[8,9], R. Claveau[12], P. Coïsson[6], M. da Silva[13], C. Davies[14], R. Deborde[6], M. Dobrovolsky[15], M. Fillion[8], C. C. Finlay[2], I. Firsov[15], A. Fournier[6], L. Gailler[16], N. Gillet[12], N. Gomez Perez[1], A. Grayver[17], K. Gwirtz[18], M. Hamoudi[4], R. Holme[19], M. Holschneider[20], G. Hulot[6], T. Jager[21], Y. Jiang[22], M. Kada[7], M. Korte[13], R. Krasnoperov[15], W. Kuang[18], D. Kudin[15], J. M. Léger[21], A. Lemgharb[4], V. Lesur[6], P. Liu[22], P. W. Livermore[14], F. D. Madsen[1,23], M Mandea[24], M. Matsushima[25], J. Matzka[13], I. Michaelis[13], T. Minami[26], M. Nair[8,9], S. Nakano[27], J-F. Oehler[28], N. Olsen[2], F. J. Pavón-Carrasco[10,11], S. Presnyakov[15], B. Qian[29], X. Rang[29], H. F. Rogers[14], M. Rother[13], D. Rouxel[28], T. Sabaka[18], S. Sato[30], J. Saynisch-Wagner[13], M. Schanner[13], M. Serrano[10,11], N. Shakespeare-Rees[14], Y. Shi[6], A. Smith[23], A. Soloviev[15,31], F. Terra-Nova[5], E. Thebault[16], L. Tøffner-Clausen[2], H. Toh[30], J. Wang[32], I. Wardinski[33], C. Watson[1], K. Whaler[23], C. Xiong[29], Q. Yan[22], Y. Yang[32], H. Yao[22], Z. Zeren[32], K. Zhang[22] and B. Zhou[32]

Abstract In November 2024, the International Association of Geomagnetism and Aeronomy (IAGA) Division V Working Group (V-MOD) adopted the fourteenth generation of the International Geomagnetic Reference Field (IGRF). This IGRF updates the previous generation with a definitive main field model for epoch 2020.0, a main field model for epoch 2025.0, and a predictive linear secular variation for 2025.0 to 2030.0. We describe the equations defining the IGRF, the spherical harmonic coefficients for this fourteenth generation model, maps of magnetic declination, inclination, and total field intensity for the model at 2025.0 and maps of the predicted rate of change of the field for the 2025.0 to 2030.0 time period.

Keywords IGRF, Magnetic field modeling, Geomagnetism

*Correspondence:
C. D. Beggan
ciar@bgs.ac.uk
Full list of author information is available at the end of the article

Graphic Abstract

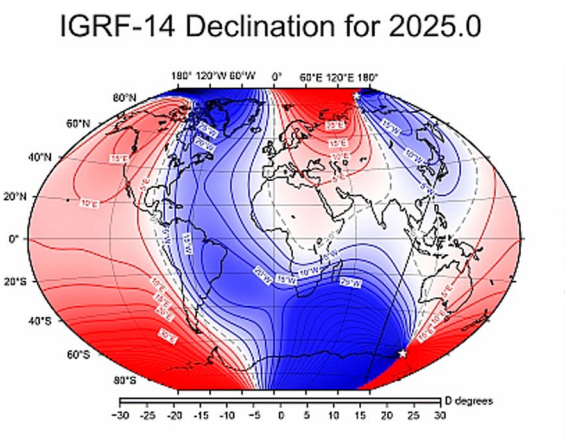

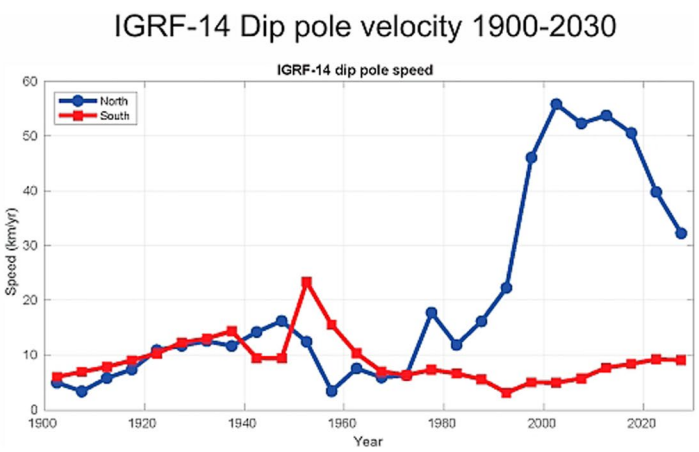

1 Introduction

The International Geomagnetic Reference Field (IGRF) is a set of spherical harmonic coefficients which describe the large-scale, time-varying portion of Earth's internal magnetic field between epochs 1900.0 A.D. and 2030.0. The IGRF is produced and maintained by an international task force of scientists under the auspices of the International Association of Geomagnetism and Aeronomy (IAGA) Working Group V-MOD (ROR: https://ror.org/013ym9476). This fourteenth generation IGRF has been derived from observations recorded by satellites, ground observatories, and magnetic surveys.

The IGRF acts as a geophysical standard reference model and is routinely used by the scientific community, for example, to study Earth's large-scale time-varying field and as a baseline to investigate local magnetic anomalies in the lithosphere. It is widely used in satellite attitude determination and control systems and other applications requiring orientation information. In the past two decades, the IGRF and its derivatives have been incorporated into space weather modeling and forecasting services.

Earth's core field changes continuously and unpredictably on timescales ranging from months to millions of years due to the chaotic nature of its generation mechanism (e.g., Aubert 2023; Hulot et al. 2010; Raphaldini et al. 2021). As secular variation can be up to ±150 nT/year in some locations, ignoring the change could incur an error of 1500 nT after a decade. In order to account for temporal changes on timescales of a few years, the IGRF is regularly revised, typically every five years to limit this error to below the sensitivity level of most users.

The latest updates to the IGRF were created from data captured at both ground observatories and from dedicated magnetic satellite missions. The temporal variation is extremely well measured by the fixed ground network while satellite data are excellent for spatial coverage globally. With the extensive availability of satellite data from the past 25 years, remote locations such as the oceans and polar regions are well characterized; though the model would certainly be improved by the addition more observatories over the oceans in the southern Pacific for example.

The IGRF models are continuous in space and have a resolution of $2\pi R_E/\sqrt{n(n+1)}$, where R_E is the Earth's radius and n is the maximum degree and order. As a spherical harmonic degree and order 13 model, the IGRF-14 has an approximate spatial resolution of 40,000 km$/\sqrt{13 \cdot 14}$ = 2965 km, i.e. around 3000 km at Earth's surface.

The modeling of the core field uses modern versions of Gauss' method for determining the internal (core and crust) part of the field from the external (ionosphere and magnetosphere) contributions. Satellite and ground observatory data captured at different altitudes are combined in this manner, reducing them to a common level at the Earth's reference radius (R_E = 6371.2 km). The technical papers from several previous generations such as Alken et al. (2021) and references therein explain the detail. The IGRF will provide valid estimates of the field from the core mantle boundary at a nominal radius of 3485 km to around 10,000 km altitude where the values of the field become small. Beggan (2022) examined the fit of the model to repeat station measurements from around the world to determine the approximate

uncertainty limits. The nominal resolution of an individual value from the model is given as 0.1 nT, though the uncertainties depend on the component of the magnetic field being evaluated.

Table 1 summarizes the current and past generations of IGRF. Each generation is composed of a set of model coefficients representing the internal time-varying geomagnetic field, which are provided in 5-year intervals. The years for which coefficients are provided are called *model epochs*. The coefficients of a certain epoch represent a snapshot of the geomagnetic field at that time, and can be labeled either as a Definitive Geomagnetic Reference Model (DGRF) or as an IGRF. DGRF models are deemed to be definitive because they have been built from the highest quality ground observatory and satellite data available from that time period and therefore are unlikely to be improved in future IGRF revisions. Models labeled as IGRF are non-definitive, and will likely be revised in the future as more data are collected and made available. DGRF models require sufficient data to compute a representative field and have only been built for the period starting in 1945. Prior to this insufficient data were available to make a high quality model so these remain labeled as IGRF. Details of the history of IGRF can be found in Barton (1997) and Macmillan and Finlay (2011). Past generations of IGRF models are archived at https://www.ncei.noaa.gov/products/international-geomagnetic-reference-field. Since later IGRFs can revise model parameters for past epochs, it is important to record which generation of IGRF was used to process a particular dataset, so that the original values can be recovered and reprocessed with the latest generation of IGRF, if needed.

In this letter, we describe the fourteenth generation of IGRF, known hereafter as IGRF-14. IGRF-14 provides a DGRF model for epoch 2020.0, an IGRF model for epoch 2025.0, and a predictive IGRF secular variation model for the 5-year time interval 2025.0–2030.0. For epochs 1900.0–2015.0, the IGRF-14 model coefficients are unchanged from IGRF-13. IGRF-14 was finalized in November 2024 by a task force of IAGA Working Group V-MOD. In the following sections, we give an overview of the IGRF model, provide the final set of IGRF-14 coefficients, and briefly discuss large-scale features of the geomagnetic field at Earth's surface as observed in the updated model.

2 Mathematical formulation of the IGRF model

The IGRF describes the main geomagnetic field $\mathbf{B}(r,\theta,\phi,t)$ which is produced by internal sources primarily inside Earth's outer core. The IGRF is valid on and above Earth's surface, where the main geomagnetic field can be described as the gradient of a scalar potential, $\mathbf{B} = -\nabla V$, and the potential function $V(r,\theta,\phi,t)$ is represented as a finite series expansion in terms of spherical harmonic coefficients, g_n^m, h_n^m, also known as the Gauss coefficients:

$$V(r,\theta,\phi,t) = a\sum_{n=1}^{N}\sum_{m=0}^{n}\left(\frac{a}{r}\right)^{n+1} \left[g_n^m(t)\cos m\phi + h_n^m(t)\sin m\phi\right]P_n^m(\cos\theta). \quad (1)$$

Here, r,θ,ϕ refer to coordinates in a geocentric spherical coordinate system, with r being radial distance from the center of the Earth, and θ,ϕ representing geocentric co-latitude and longitude, respectively. A reference radius

Table 1 Summary of IGRF generations, validity periods, release years, and references

Full name	Short name	Validity period	Definitive period	Release year	Reference
IGRF 14th generation	IGRF-14	1900.0–2030.0	1945.0–2020.0	2024	This paper
IGRF 13th generation	IGRF-13	1900.0–2025.0	1945.0–2015.0	2019	Alken et al. (2021)
IGRF 12th generation	IGRF-12	1900.0–2020.0	1945.0–2010.0	2014	Thébault et al. (2015)
IGRF 11th generation	IGRF-11	1900.0–2015.0	1945.0–2005.0	2009	Finlay et al. (2010a)
IGRF 10th generation	IGRF-10	1900.0–2010.0	1945.0–2000.0	2004	Maus et al. (2005); Macmillan and Maus (2005)
IGRF 9th generation	IGRF-9	1900.0–2005.0	1945.0–2000.0	2003	Macmillan et al. (2003)
IGRF 8th generation	IGRF-8	1900.0–2005.0	1945.0–1990.0	1999	Mandea and Macmillan (2000)
IGRF 7th generation	IGRF-7	1900.0–2000.0	1945.0–1990.0	1995	Barton (1997)
IGRF 6th generation	IGRF-6	1945.0–1995.0	1945.0–1985.0	1991	Langel (1992)
IGRF 5th generation	IGRF-5	1945.0–1990.0	1945.0–1980.0	1987	Barraclough et al. (1987); Langel et al. (1988)
IGRF 4th generation	IGRF-4	1945.0–1990.0	1965.0–1980.0	1985	Barraclough (1987)
IGRF 3rd generation	IGRF-3	1965.0–1985.0	1965.0–1975.0	1981	Peddie (1982)
IGRF 2nd generation	IGRF-2	1955.0–1980.0	–	1975	IAGA Division I Study Group (1975)
IGRF 1st generation	IGRF-1	1955.0–1975.0	–	1968	Cain and Cain (1971); Zmuda (1971a, 1971b)

$a = 6371.2$ km is chosen to approximate the mean Earth radius. Temporal changes are denoted by t. The $P_n^m(\cos\theta)$ are Schmidt semi-normalized associated Legendre functions of degree n and order m (e.g., Winch et al. 2005). The parameter N specifies the maximum spherical harmonic degree of expansion, and was chosen to be 10 up to and including epoch 1995, after which it increases to 13 to account for the smaller scale internal signals which can be captured by high-resolution satellite missions such as Ørsted, CHAMP and Swarm. The Gauss coefficients $g_n^m(t), h_n^m(t)$ change in time and are provided in units of nanoTesla (nT) in IGRF-14 at 5-year epoch intervals. The time dependence of these parameters is modeled as piecewise linear, and is given by:

$$g_n^m(t) = g_n^m(T_t) + (t - T_t)\dot{g}_n^m(T_t), \tag{2}$$

$$h_n^m(t) = h_n^m(T_t) + (t - T_t)\dot{h}_n^m(T_t), \tag{3}$$

where $g_n^m(T_t), h_n^m(T_t)$ are the Gauss coefficients at epoch T_t (in years), which immediately precedes time t (also in years). The model epochs in IGRF-14 are provided in exact multiples of 5 years starting in 1900 and ending in 2025 (see Table 2), so that $T_t \leq t < T_t + 5$. For $T_t < 2025$, the parameters $\dot{g}_n^m(T_t), \dot{h}_n^m(T_t)$ represent the linear approximation to the change in the Gauss coefficients over the 5 year interval spanning $[T_t, T_t + 5]$. They may be computed in units of nanoTesla per year (nT/year) as:

$$\dot{g}_n^m(T_t) = \frac{1}{5}\big(g_n^m(T_t + 5) - g_n^m(T_t)\big), \tag{4}$$

$$\dot{h}_n^m(T_t) = \frac{1}{5}\big(h_n^m(T_t + 5) - h_n^m(T_t)\big). \tag{5}$$

The main field coefficients are not yet known for $T_t = 2030$, and so for the final 5 years of model validity (2025–2030 for IGRF-14), the coefficients $\dot{g}_n^m(2025), \dot{h}_n^m(2025)$ are explicitly provided (see last column of Table 2) in units of nT/year. Details on the individual candidate secular variation forecasts and the procedure used to combine them into a final set of $\dot{g}_n^m(2025), \dot{h}_n^m(2025)$ may be found in Beggan et al. (2026) and references therein.

3 The 14th generation IGRF

In July 2023, during an IAGA V-MOD Working Group meeting held in Berlin, Germany, a task force of volunteer geomagnetic modelers was assembled to oversee the call for IGRF-14 candidate models and their evaluation. In March 2024, the task force issued an international call for three candidates:

- a DGRF main field model for the epoch 2020.0,
- an IGRF main field model for the epoch 2025.0,
- an IGRF linear secular variation model for the time period 2025.0–2030.0.

Nineteen teams representing 27 international institutes responded to the call. The number of teams and institutions who participated in IGRF-14 exceeded that of any previous generation. The task force received 14 DGRF main field candidates for epoch 2020.0, 15 IGRF main field candidates for 2025.0, and 18 IGRF secular variation candidates for 2025.0–2030.0. Following recent IGRF conventions, the main field candidates for IGRF-14 describe the spatial variation of the field to a maximum spherical harmonic degree and order of 13, while the secular variation candidates extend to a maximum degree and order of 8. Each of the 19 teams was managed by a team leader from the *lead institution*, and many teams also included personnel from supporting institutions.

The 19 lead institutions for IGRF-14 are: (1) British Geological Survey (United Kingdom), (2) Technical University of Denmark (Denmark), (3) National Institute of Natural Hazards (China), (4) Universidad Complutense de Madrid (Spain), (5) University of Colorado Boulder (United States), (6) GFZ Helmholtz Centre for Geosciences (Germany), (7) Institut de physique du globe de Paris (France), (8) Institut des Sciences de la Terre (France), (9) Geophysical Center of the Russian Academy of Sciences (Russia), (10) Kyoto University (Japan), (11) University of Leeds (United Kingdom), (12) University of Edinburgh (United Kingdom), (13) NASA Goddard Space Flight Center (United States), (14) Université de Strasbourg (France), (15) Technical University of Berlin (Germany), (16) Macau Institute of Space Technology and Application (China), (17) Wuhan University (China), (18) Observatoire de Physique du Globe de Clermont Ferrand (France) and (19) University of Science and Technology Houari Boumediene (Algeria). Further details of their submissions are described in Beggan et al. (2026).

Some of the lead institutes listed above also acted as supporting institutions to other teams. The supporting institutes which are not listed above include: The Institute of Statistical Mathematics (Japan), Institute of Science Tokyo (Japan), Nantes Université (France), University of Tokyo (Japan), CEA-Leti (France), University of Grenoble (France), SHOM (France) and University of Liverpool (UK).

Data recorded by the Swarm satellite mission (Friis-Christensen et al. 2006) and the ground observatory network (see Table 4) played a crucial role in the development of many of the IGRF-14 candidate models. Swarm ASM-V experimental data from the CNES-funded

Table 2 14th generation International Geomagnetic Reference Field

	deg	ord	IGRF	IGRF	IGRF	IGRF	IGRF	IGRF	IGRF	IGRF	IGRF	DGRF	DGRF	DGRF	DGRF	DGRF	DGRF	DGRF	DGRF	DGRF	DGRF	DGRF	DGRF	DGRF	DGRF	DGRF	IGRF	SV
g/hn		m	1900	1905	1910	1915	1920	1925	1930	1935	1940	1945	1950	1955	1960	1965	1970	1975	1980	1985	1990	1995	2000	2005	2010	2015	2020	2025	25–30
g	1	0	−31543	−31464	−31354	−31212	−31060	−30926	−30805	−30715	−30654	−30594	−30554	−30500	−30421	−30334	−30220	−30100	−29992	−29873	−29775	−29692	−29619.4	−29554.63	−29496.57	−29441.46	−29403.41	−29350.0	12.6
g	1	1	−2298	−2298	−2297	−2306	−2317	−2318	−2316	−2306	−2292	−2285	−2250	−2215	−2169	−2119	−2068	−2013	−1956	−1905	−1848	−1784	−1728.2	−1669.05	−1586.42	−1501.77	−1451.37	−1410.3	10.0
h	1	1	5922	5909	5898	5875	5845	5817	5808	5812	5821	5810	5815	5820	5791	5776	5737	5675	5604	5500	5406	5306	5186.1	5077.99	4944.26	4795.99	4653.35	4545.5	−21.5
g	2	0	−677	−728	−769	−802	−839	−893	−951	−1018	−1106	−1244	−1341	−1440	−1555	−1662	−1781	−1902	−1997	−2072	−2131	−2200	−2267.7	−2337.24	−2396.06	−2445.88	−2499.78	−2556.2	−11.2
g	2	1	2905	2928	2948	2956	2959	2969	2980	2984	2981	2990	2998	3003	3002	2997	3000	3010	3027	3044	3059	3070	3068.4	3047.69	3026.34	3012.2	2981.96	2950.9	−5.3
h	2	1	−1061	−1086	−1128	−1191	−1259	−1334	−1424	−1520	−1614	−1702	−1810	−1898	−1967	−2016	−2047	−2067	−2129	−2197	−2279	−2366	−2481.6	−2594.50	−2708.54	−2845.41	−2991.72	−3133.6	−27.3
g	2	2	924	1041	1176	1309	1407	1471	1517	1550	1566	1578	1576	1581	1590	1594	1611	1632	1663	1687	1686	1681	1670.9	1657.76	1668.17	1676.35	1676.85	1648.7	−8.3
h	2	2	1121	1065	1000	917	823	728	644	586	528	477	381	291	206	114	25	−68	−200	−306	−373	−413	−458.0	−515.43	−575.73	−642.17	−734.62	−814.2	−11.1
g	3	0	1022	1037	1058	1084	1111	1140	1172	1206	1240	1282	1297	1302	1302	1297	1287	1276	1281	1296	1314	1335	1339.6	1336.30	1339.85	1350.33	1363.00	1360.9	−1.5
g	3	1	−1469	−1494	−1524	−1559	−1600	−1645	−1692	−1740	−1790	−1834	−1889	−1944	−1992	−2038	−2091	−2144	−2180	−2208	−2239	−2267	−2288.0	−2305.83	−2326.54	−2352.26	−2380.80	−2404.2	−4.4
h	3	1	−330	−357	−389	−421	−445	−462	−480	−494	−499	−499	−476	−462	−414	−404	−366	−333	−336	−310	−284	−262	−227.6	−198.86	−160.40	−115.29	−81.96	−56.9	3.8
g	3	2	1256	1239	1223	1212	1205	1202	1205	1215	1232	1255	1274	1288	1289	1292	1278	1260	1251	1247	1248	1249	1252.1	1246.39	1232.10	1225.85	1236.06	1243.8	0.4
h	3	2	3	34	62	84	103	119	133	146	163	186	206	216	224	240	251	262	271	284	293	302	293.4	269.72	251.75	245.04	241.80	237.6	−0.2
g	3	3	572	635	705	778	839	881	907	918	916	913	896	882	878	856	838	830	833	829	802	759	714.5	672.51	633.73	581.69	525.60	453.4	−15.6
h	3	3	523	480	425	360	293	229	166	101	43	−11	−46	−83	−130	−165	−196	−223	−252	−297	−352	−427	−491.1	−524.72	−537.03	−538.7	−542.52	−549.6	−3.9
g	4	0	876	880	884	887	889	891	896	903	914	944	954	958	957	957	952	946	938	936	939	940	932.3	920.55	912.66	907.42	902.82	894.7	−1.7
g	4	1	628	643	660	678	695	711	727	744	762	776	792	796	800	804	800	791	782	780	780	780	786.8	797.96	808.97	813.68	809.47	799.6	−2.3
h	4	1	195	203	211	218	220	216	205	188	169	144	136	133	135	148	167	191	212	232	247	262	272.6	282.07	286.48	283.54	282.10	278.6	−1.3
g	4	2	660	653	644	631	616	601	584	565	550	544	528	510	504	479	461	438	398	361	325	290	250.0	210.65	166.58	120.49	86.18	55.8	−5.8
h	4	2	−69	−77	−90	−109	−134	−163	−195	−226	−252	−276	−278	−274	−278	−269	−266	−265	−257	−249	−240	−236	−231.9	−225.23	−211.03	−188.43	−158.50	−134.0	4.1
g	4	3	−361	−380	−400	−416	−424	−426	−422	−415	−405	−421	−408	−397	−394	−390	−395	−405	−419	−424	−423	−418	−403.0	−379.86	−356.83	−334.85	−309.47	−281.1	5.4
h	4	3	−210	−201	−189	−173	−153	−130	−109	−90	−72	−55	−37	−23	3	13	26	39	53	69	84	97	119.8	145.15	164.46	180.95	199.75	212.0	1.6
g	4	4	134	146	160	178	199	217	234	249	265	304	303	290	269	252	234	216	199	170	141	122	111.3	100.00	89.40	70.38	47.44	12.0	−6.8
h	4	4	−75	−65	−55	−51	−57	−70	−90	−114	−141	−178	−210	−230	−255	−269	−279	−288	−297	−297	−299	−306	−303.8	−305.36	−309.72	−329.23	−350.30	−375.4	−4.1
g	5	0	−184	−192	−201	−211	−221	−230	−237	−241	−241	−253	−240	−229	−222	−219	−216	−218	−218	−214	−214	−214	−218.8	−227.00	−230.87	−232.91	−234.42	−232.9	0.6
g	5	1	328	328	327	327	326	326	327	329	334	346	349	360	362	358	359	356	357	355	353	352	351.4	354.41	357.29	360.14	363.26	369.0	1.3
h	5	1	−210	−193	−172	−148	−122	−96	−72	−51	−33	−12	3	15	16	19	26	31	46	47	46	46	43.8	42.72	44.58	46.98	47.52	45.3	−0.5
g	5	2	264	259	253	245	236	226	218	211	208	194	211	230	242	254	262	264	261	253	245	235	222.3	208.95	200.26	192.35	187.86	187.2	0.0
h	5	2	53	56	57	58	58	58	60	64	71	95	103	110	125	128	139	148	150	150	154	165	171.9	180.25	189.01	196.98	208.36	220.0	2.1
g	5	3	5	−1	−9	−16	−23	−28	−32	−33	−33	−20	−20	−23	−26	−31	−42	−59	−74	−93	−109	−118	−130.4	−136.54	−141.05	−140.94	−140.73	−138.7	0.7
h	5	3	−33	−32	−33	−34	−38	−44	−53	−64	−75	−67	−87	−98	−117	−126	−139	−152	−151	−154	−153	−143	−133.1	−123.45	−118.06	−119.14	−121.43	−122.9	0.5
g	5	4	−86	−93	−102	−111	−119	−125	−131	−136	−141	−142	−147	−152	−156	−157	−160	−159	−162	−164	−165	−166	−168.6	−168.05	−163.17	−157.4	−151.16	−141.9	2.3
h	5	4	−124	−125	−126	−126	−125	−122	−118	−115	−113	−119	−122	−121	−114	−97	−91	−83	−78	−75	−69	−55	−39.3	−19.57	−0.01	15.98	32.09	42.9	1.7
g	5	5	−16	−26	−38	−51	−62	−69	−74	−76	−76	−82	−76	−69	−63	−62	−56	−49	−48	−46	−36	−17	−12.9	−13.55	−8.03	4.3	13.98	20.9	1.0
h	5	5	3	11	21	32	43	51	58	64	69	82	80	78	81	81	83	88	92	95	97	107	106.3	103.85	101.04	100.12	99.14	106.2	1.9
g	6	0	63	62	62	61	61	61	60	59	57	59	54	47	46	45	43	45	48	53	61	68	72.3	73.60	72.78	69.55	65.97	64.3	−0.2
g	6	1	61	60	58	57	55	54	53	53	54	57	57	57	58	61	64	66	66	65	65	67	68.2	69.56	68.69	67.57	65.56	63.8	−0.3
h	6	1	−9	−7	−5	−2	0	3	4	4	4	6	−1	−9	−10	−11	−12	−13	−15	−16	−16	−17	−17.4	−20.33	−20.90	−20.61	−19.22	−18.4	0.3
g	6	2	−11	−11	−11	−10	−10	−9	−9	−8	−7	6	4	3	1	8	15	28	42	51	59	68	74.2	76.74	75.92	72.79	72.96	76.7	0.8
h	6	2	83	86	89	93	96	99	102	104	105	100	99	96	99	100	100	99	93	88	82	72	63.7	54.75	44.18	33.3	25.02	16.8	−1.6
g	6	3	−217	−221	−224	−228	−233	−238	−242	−246	−249	−246	−247	−247	−237	−228	−212	−198	−192	−185	−178	−170	−160.9	−151.34	−141.40	−129.85	−121.57	−115.7	1.2

Table 2 (continued)

	deg	ord	IGRF	IGRF	IGRF	IGRF	IGRF	IGRF	IGRF	IGRF	IGRF	DGRF	DGRF	DGRF	DGRF	DGRF	DGRF	DGRF	DGRF	DGRF	DGRF	DGRF	DGRF	DGRF	DGRF	IGRF	SV
h	6	3	2	4	5	8	11	14	19	25	33	16	33	48	60	68	72	75	71	69	69	67	65.1	63.63	61.54	58.74	52.76	48.9	−0.4
g	6	4	−58	−57	−54	−51	−46	−40	−32	−25	−18	−25	−16	−8	−1	4	2	1	4	4	3	−1	−5.9	−14.58	−22.83	−28.93	−36.06	−40.9	−0.8
h	6	4	−35	−32	−29	−26	−22	−18	−16	−15	−15	−9	−12	−16	−20	−32	−37	−41	−43	−48	−52	−58	−61.2	−63.53	−66.26	−66.64	−64.40	−59.8	0.8
g	6	5	59	57	54	49	44	39	32	25	18	21	12	7	−2	1	3	6	14	16	18	19	16.9	14.58	13.10	13.14	13.60	14.9	0.4
h	6	5	36	32	28	23	18	13	8	4	0	−16	−12	−12	−11	−8	−6	−4	−2	−1	1	1	0.7	0.24	3.02	7.35	8.96	10.9	0.7
g	6	6	−90	−92	−95	−98	−101	−103	−104	−106	−107	−104	−105	−107	−113	−111	−112	−111	−108	−102	−96	−93	−90.4	−86.36	−78.09	−70.85	−64.80	−60.8	0.9
h	6	6	−69	−67	−65	−62	−57	−52	−46	−40	−33	−39	−30	−24	−17	−7	1	11	17	21	24	36	43.8	50.94	55.40	62.41	68.04	72.8	0.9
g	7	0	70	70	71	72	73	73	74	74	74	70	65	65	67	75	72	71	72	74	77	77	79.0	79.88	80.44	81.29	80.54	79.6	−0.1
g	7	1	−55	−54	−54	−54	−54	−54	−54	−53	−53	−40	−55	−56	−56	−57	−57	−56	−59	−62	−64	−72	−74.0	−74.46	−75.00	−75.99	−76.63	−76.9	−0.1
h	7	1	−45	−46	−47	−48	−49	−50	−51	−52	−52	−45	−35	−50	−55	−61	−70	−77	−82	−83	−80	−69	−64.6	−61.14	−57.80	−54.27	−51.50	−48.9	0.6
g	7	2	0	0	1	2	2	3	4	4	4	0	2	2	5	4	1	1	2	3	2	1	0.0	−1.65	−4.55	−6.79	−8.23	−8.8	−0.1
h	7	2	−13	−14	−14	−14	−14	−14	−15	−17	−18	−18	−17	−24	−28	−27	−27	−26	−27	−27	−26	−25	−24.2	−22.57	−21.20	−19.53	−16.85	−14.4	0.5
g	7	3	34	33	32	31	29	27	25	23	20	0	1	10	15	13	14	16	21	24	26	28	33.3	38.73	45.24	51.82	56.45	59.3	0.5
h	7	3	−10	−11	−12	−12	−13	−14	−14	−14	−14	2	0	−4	−6	−2	−4	−5	−5	−2	0	4	6.2	6.82	6.54	5.59	2.36	−1.0	−0.7
g	7	4	−41	−41	−40	−38	−37	−35	−34	−33	−31	−29	−40	−32	−32	−26	−22	−14	−12	−6	−1	5	9.1	12.30	14.00	15.07	15.80	15.8	−0.1
h	7	4	−1	0	1	2	4	5	6	7	7	6	10	8	7	6	8	10	16	20	21	24	24.0	25.35	24.96	24.45	23.56	23.5	0.0
g	7	5	−21	−20	−19	−18	−16	−14	−12	−11	−9	−10	−7	−11	−7	−6	−2	0	1	4	5	4	6.9	9.37	10.46	9.32	6.30	2.5	−0.8
h	7	5	28	28	28	28	28	29	29	29	29	28	36	28	23	26	23	22	18	17	17	17	14.8	10.93	7.03	3.27	−2.19	−7.4	−0.9
g	7	6	18	18	18	19	19	19	18	18	17	15	5	9	17	13	13	12	11	10	9	8	7.3	5.42	1.64	−2.88	−7.21	−11.2	−0.8
h	7	6	−12	−12	−13	−15	−16	−17	−18	−19	−20	−17	−18	−20	−18	−23	−23	−23	−23	−23	−23	−24	−25.4	−26.32	−27.61	−27.5	−27.19	−25.1	0.5
g	7	7	6	6	6	6	6	6	6	6	5	29	19	18	8	1	−2	−5	−2	0	0	−2	−1.2	1.94	4.92	6.61	9.77	14.3	0.9
h	7	7	−22	−22	−22	−22	−22	−21	−20	−19	−19	−22	−16	−18	−17	−12	−11	−12	−10	−7	−4	−6	−5.8	−4.64	−3.28	−2.32	−1.90	−2.2	−0.3
g	8	0	11	11	11	11	11	11	11	11	11	13	22	11	15	13	14	14	18	21	23	25	24.4	24.80	24.41	23.98	23.66	23.1	−0.1
g	8	1	8	8	8	8	7	7	7	7	7	7	15	9	6	5	6	6	6	6	5	6	6.6	7.62	8.21	8.89	9.74	10.9	0.2
h	8	1	8	8	8	8	8	8	8	8	8	12	5	10	11	7	7	6	7	8	10	11	11.9	11.20	10.84	10.04	8.43	7.2	−0.3
g	8	2	−4	−4	−4	−4	−3	−3	−3	−3	−3	−8	−4	−6	−4	−4	−2	−1	0	0	−1	−6	−9.2	−11.73	−14.50	−16.78	−17.49	−17.5	0.0
h	8	2	−14	−15	−15	−15	−15	−15	−15	−15	−14	−21	−22	−15	−14	−12	−15	−16	−18	−19	−19	−21	−21.5	−20.88	−20.03	−18.26	−15.23	−12.6	0.4
g	8	3	−9	−9	−9	−9	−9	−9	−9	−9	−10	−5	−1	−14	−11	−14	−13	−12	−11	−11	−10	−9	−7.9	−6.88	−5.59	−3.16	−0.49	2.0	0.4
h	8	3	7	7	6	6	6	6	5	5	5	−12	0	5	7	9	6	4	4	5	6	8	8.5	9.83	11.83	13.18	12.83	11.5	−0.3
g	8	4	1	1	1	2	2	2	2	1	1	9	11	6	2	0	−3	−8	−7	−9	−12	−14	−16.6	−18.11	−19.34	−20.56	−21.07	−21.8	−0.1
h	8	4	−13	−13	−13	−13	−14	−14	−14	−15	−15	−7	−21	−23	−18	−16	−17	−19	−22	−23	−22	−23	−21.5	−19.71	−17.41	−14.6	−11.76	−9.7	0.4
g	8	5	2	2	2	3	4	4	5	6	6	7	15	10	10	8	5	4	4	4	3	9	9.1	10.17	11.61	13.33	15.28	16.9	0.3
h	8	5	5	5	5	5	5	5	5	5	5	2	−8	3	4	4	6	6	9	11	12	15	15.5	16.22	16.71	16.16	14.94	12.7	−0.5
g	8	6	−9	−8	−8	−8	−7	−7	−6	−6	−5	−10	−13	−7	−5	−1	0	0	3	4	4	6	7.0	9.36	10.85	11.76	13.65	14.9	0.1
h	8	6	16	16	16	16	17	17	18	18	19	18	17	23	23	24	21	18	16	14	12	11	8.9	7.61	6.96	5.69	3.62	0.7	−0.6
g	8	7	5	5	5	6	6	7	8	8	9	7	5	6	10	11	11	10	6	4	2	−5	−7.9	−11.25	−14.05	−15.98	−16.59	−16.8	0.0
h	8	7	−5	−5	−5	−5	−5	−5	−5	−5	−5	3	−4	−4	1	−3	−6	−10	−13	−15	−16	−16	−14.9	−12.76	−10.74	−9.1	−6.90	−5.2	0.3
g	8	8	8	8	8	8	8	8	8	7	7	2	−1	9	8	4	3	1	−1	−4	−6	−7	−7.0	−4.87	−3.54	−2.02	−0.34	1.0	0.3
h	8	8	−18	−18	−18	−18	−19	−19	−19	−19	−19	−11	−17	−13	−20	−17	−16	−17	−15	−11	−10	−4	−2.1	−0.06	1.64	2.26	2.90	3.9	0.2
g	9	0	8	8	8	8	8	8	8	8	8	5	3	4	4	8	8	7	5	5	4	4	5.0	5.58	5.50	5.33	5.03	4.7	–
g	9	1	10	10	10	10	10	10	10	10	10	−21	−7	9	6	10	10	10	10	10	9	9	9.4	9.76	9.45	8.83	8.36	8.0	–
h	9	1	−20	−20	−20	−20	−20	−20	−20	−20	−21	−27	−24	−11	−18	−22	−21	−21	−21	−21	−20	−20	−19.7	−20.11	−20.54	−21.77	−23.44	−24.8	–

Table 2 (continued)

	deg	ord	IGRF	IGRF	IGRF	IGRF	IGRF	IGRF	IGRF	IGRF	IGRF	DGRF	DGRF	DGRF	DGRF	DGRF	DGRF	DGRF	DGRF	DGRF	DGRF	DGRF	DGRF	DGRF	DGRF	IGRF	SV	
g	9	2	1	1	1	1	1	1	1	1	1	1	−1	−4	0	2	2	2	1	1	1	3	3.0	3.58	3.45	3.02	2.84	3.0	–
h	9	2	14	14	14	14	14	14	14	15	15	17	19	12	12	15	16	16	16	15	15	15	13.4	12.69	11.51	10.76	11.04	12.1	–
g	9	3	−11	−11	−11	−11	−11	−11	−12	−12	−12	−11	−25	−5	−9	−13	−12	−12	−12	−12	−12	−10	−8.4	−6.94	−5.27	−3.22	−1.48	−0.2	–
h	9	3	5	5	5	5	5	5	5	5	5	29	12	7	2	7	6	7	9	9	11	12	12.5	12.67	12.75	11.74	9.86	8.3	–
g	9	4	12	12	12	12	12	12	12	11	11	3	10	2	1	10	10	10	9	9	9	8	6.3	5.01	3.13	0.67	−1.14	−2.5	–
h	9	4	−3	−3	−3	−3	−3	−3	−3	−3	−3	−9	2	6	0	−4	−4	−4	−5	−6	−7	−6	−6.2	−6.72	−7.14	−6.74	−5.13	−3.4	–
g	9	5	1	1	1	1	1	1	1	1	1	16	5	4	4	−1	−1	−1	−3	−3	−4	−8	−8.9	−10.76	−12.38	−13.2	−13.22	−13.1	–
h	9	5	−2	−2	−2	−2	−2	−2	−2	−3	−3	4	2	−2	−3	−5	−5	−5	−6	−6	−7	−8	−8.4	−8.16	−7.42	−6.88	−6.20	−5.3	–
g	9	6	−2	−2	−2	−2	−2	−2	−2	−2	−2	−3	−5	1	−1	−1	0	−1	−1	−1	−2	−1	−1.5	−1.25	−0.76	−0.1	1.08	2.4	–
h	9	6	8	8	8	8	9	9	9	9	9	9	8	10	9	10	10	10	9	9	9	8	8.4	8.10	7.97	7.79	7.79	7.2	–
g	9	7	2	2	2	2	2	2	3	3	3	−4	−2	2	−2	5	3	4	7	7	7	10	9.3	8.76	8.43	8.68	8.82	8.6	–
h	9	7	10	10	10	10	10	10	10	11	11	6	8	7	8	10	11	11	10	9	8	5	3.8	2.92	2.14	1.04	0.40	−0.6	–
g	9	8	−1	0	0	0	0	0	0	0	1	−3	3	2	3	1	1	1	2	1	1	−2	−4.3	−6.66	−8.42	−9.06	−9.23	−8.7	–
h	9	8	−2	−2	−2	−2	−2	−2	−2	−2	−2	1	−11	−6	0	−4	−2	−3	−6	−7	−7	−8	−8.2	−7.73	−6.08	−3.89	−1.44	0.8	–
g	9	9	−1	−1	−1	−1	−1	−1	−2	−2	−2	−4	8	5	−1	−2	−1	−2	−5	−5	−6	−8	−8.2	−9.22	−10.08	−10.54	−11.86	−12.8	–
h	9	9	2	2	2	2	2	2	2	2	2	8	−7	5	5	1	1	1	2	2	2	3	4.8	6.01	7.01	8.44	9.60	9.8	–
g	10	0	−3	−3	−3	−3	−3	−3	−3	−3	−3	−3	−8	−3	1	−2	−3	−3	−4	−4	−3	−3	−2.6	−2.17	−1.94	−2.01	−1.84	−1.3	–
g	10	1	−4	−4	−4	−4	−4	−4	−4	−4	−4	11	4	−5	−3	−3	−3	−3	−4	−4	−4	−6	−6.0	−6.12	−6.24	−6.26	−6.25	−6.4	–
h	10	1	2	2	2	2	2	2	2	2	2	5	13	−4	4	2	1	1	1	1	2	1	1.7	2.19	2.73	3.28	3.38	3.3	–
g	10	2	2	2	2	2	2	2	2	2	2	1	−1	−1	4	2	2	2	2	3	2	2	1.7	1.42	0.89	0.17	−0.11	0.2	–
h	10	2	1	1	1	1	1	1	1	1	1	1	−2	0	1	1	1	1	0	0	1	0	0.0	0.10	−0.10	−0.4	−0.18	0.1	–
g	10	3	−5	−5	−5	−5	−5	−5	−5	−5	−5	2	13	2	0	−5	−5	−5	−5	−5	−5	−4	−3.1	−2.35	−1.07	0.55	1.66	2.0	–
h	10	3	2	2	2	2	2	2	2	2	2	−20	−10	−8	0	2	3	3	3	3	3	4	4.0	4.46	4.71	4.55	3.50	2.5	–
g	10	4	−2	−2	−2	−2	−2	−2	−2	−2	−2	−5	−4	−3	−1	−2	−1	−2	−2	−2	−2	−1	−0.5	−0.15	−0.16	−0.55	−0.86	−1.0	–
h	10	4	6	6	6	6	6	6	6	6	6	−1	2	−2	2	6	4	4	6	6	6	5	4.9	4.76	4.44	4.4	4.86	5.4	–
g	10	5	6	6	6	6	6	6	6	6	6	−1	4	7	4	4	6	5	5	5	4	4	3.7	3.06	2.45	1.7	0.65	−0.5	–
h	10	5	−4	−4	−4	−4	−4	−4	−4	−4	−4	−6	−3	−4	−5	−4	−4	−4	−4	−4	−4	−5	−5.9	−6.58	−7.22	−7.92	−8.62	−9.0	–
g	10	6	4	4	4	4	4	4	4	4	4	8	12	4	6	4	4	4	3	3	3	2	1.0	0.29	−0.33	−0.67	−0.88	−0.9	–
h	10	6	0	0	0	0	0	0	0	0	0	6	6	1	1	0	0	−1	0	0	0	−1	−1.2	−1.01	−0.96	−0.61	−0.11	0.4	–
g	10	7	0	0	0	0	0	0	0	0	0	−1	3	−2	1	0	1	1	1	1	1	2	2.0	2.06	2.13	2.13	1.88	1.5	–
h	10	7	−2	−2	−2	−2	−2	−2	−2	−1	−1	−4	−3	−3	−1	−2	−1	−1	−1	−1	−2	−2	−2.9	−3.47	−3.95	−4.16	−4.26	−4.2	–
g	10	8	2	2	2	1	1	1	1	2	2	−3	2	6	−1	2	0	0	2	2	3	5	4.2	3.77	3.09	2.33	1.44	0.9	–
h	10	8	4	4	4	4	4	4	4	4	4	−2	6	7	6	3	3	3	4	4	3	1	0.2	−0.86	−1.99	−2.85	−3.43	−3.8	–
g	10	9	2	2	2	2	3	3	3	3	3	5	10	−2	2	2	3	3	3	3	3	1	0.3	−0.21	−1.03	−1.8	−2.38	−2.6	–
h	10	9	0	0	0	0	0	0	0	0	0	0	11	−1	0	0	1	1	0	0	−1	−2	−2.2	−2.31	−1.97	−1.12	−0.10	0.9	–
g	10	10	0	0	0	0	0	0	0	0	0	−2	3	0	0	0	−1	−1	0	0	0	0	−1.1	−2.09	−2.80	−3.59	−3.84	−3.9	–
h	10	10	−6	−6	−6	−6	−6	−6	−6	−6	−6	−2	8	−3	−7	−6	−4	−5	−6	−6	−6	−7	−7.4	−7.93	−8.31	−8.72	−8.84	−9.0	–
g	11	0	–	–	–	–	–	–	–	–	–	–	–	–	–	–	–	–	–	–	–	–	2.7	2.95	3.05	3	2.96	3.0	–
g	11	1	–	–	–	–	–	–	–	–	–	–	–	–	–	–	–	–	–	–	–	–	−1.7	−1.60	−1.48	−1.4	−1.36	−1.4	–
h	11	1	–	–	–	–	–	–	–	–	–	–	–	–	–	–	–	–	–	–	–	–	0.1	0.26	0.13	0	−0.02	0.0	–
g	11	2	–	–	–	–	–	–	–	–	–	–	–	–	–	–	–	–	–	–	–	–	−1.9	−1.88	−2.03	−2.3	−2.51	−2.5	–
h	11	2	–	–	–	–	–	–	–	–	–	–	–	–	–	–	–	–	–	–	–	–	1.3	1.44	1.67	2.11	2.50	2.8	–

Table 2 (continued)

	deg	ord	IGRF	IGRF	IGRF	IGRF	IGRF	IGRF	IGRF	IGRF	IGRF	DGRF	DGRF	DGRF	DGRF	DGRF	DGRF	DGRF	DGRF	DGRF	DGRF	DGRF	DGRF	DGRF	DGRF	DGRF	IGRF	SV
g	11	3	–	–	–	–	–	–	–	–	–	–	–	–	–	–	–	–	–	–	–	–	1.5	1.44	1.65	2.08	2.31	2.4	–
h	11	3	–	–	–	–	–	–	–	–	–	–	–	–	–	–	–	–	–	–	–	–	− 0.9	− 0.77	− 0.66	− 0.6	− 0.55	− 0.6	–
g	11	4	–	–	–	–	–	–	–	–	–	–	–	–	–	–	–	–	–	–	–	–	− 0.1	− 0.31	− 0.51	− 0.79	− 0.85	− 0.6	–
h	11	4	–	–	–	–	–	–	–	–	–	–	–	–	–	–	–	–	–	–	–	–	− 2.6	− 2.27	− 1.76	− 1.05	− 0.39	0.1	–
g	11	5	–	–	–	–	–	–	–	–	–	–	–	–	–	–	–	–	–	–	–	–	0.1	0.29	0.54	0.58	0.28	0.0	–
h	11	5	–	–	–	–	–	–	–	–	–	–	–	–	–	–	–	–	–	–	–	–	0.9	0.90	0.85	0.76	0.62	0.5	–
g	11	6	–	–	–	–	–	–	–	–	–	–	–	–	–	–	–	–	–	–	–	–	− 0.7	− 0.79	− 0.79	− 0.7	− 0.66	− 0.6	–
h	11	6	–	–	–	–	–	–	–	–	–	–	–	–	–	–	–	–	–	–	–	–	− 0.7	− 0.58	− 0.39	− 0.2	− 0.21	− 0.3	–
g	11	7	–	–	–	–	–	–	–	–	–	–	–	–	–	–	–	–	–	–	–	–	0.7	0.53	0.37	0.14	− 0.07	− 0.1	–
h	11	7	–	–	–	–	–	–	–	–	–	–	–	–	–	–	–	–	–	–	–	–	− 2.8	− 2.69	− 2.51	− 2.12	− 1.66	− 1.2	–
g	11	8	–	–	–	–	–	–	–	–	–	–	–	–	–	–	–	–	–	–	–	–	1.7	1.80	1.79	1.7	1.44	1.1	–
h	11	8	–	–	–	–	–	–	–	–	–	–	–	–	–	–	–	–	–	–	–	–	− 0.9	− 1.08	− 1.27	− 1.44	− 1.60	− 1.7	–
g	11	9	–	–	–	–	–	–	–	–	–	–	–	–	–	–	–	–	–	–	–	–	0.1	0.16	0.12	− 0.22	− 0.59	− 1.0	–
h	11	9	–	–	–	–	–	–	–	–	–	–	–	–	–	–	–	–	–	–	–	–	− 1.2	− 1.58	− 2.11	− 2.57	− 2.98	− 2.9	–
g	11	10	–	–	–	–	–	–	–	–	–	–	–	–	–	–	–	–	–	–	–	–	1.2	0.96	0.75	0.44	0.18	− 0.1	–
h	11	10	–	–	–	–	–	–	–	–	–	–	–	–	–	–	–	–	–	–	–	–	− 1.9	− 1.90	− 1.94	− 2.01	− 1.97	− 1.8	–
g	11	11	–	–	–	–	–	–	–	–	–	–	–	–	–	–	–	–	–	–	–	–	4.0	3.99	3.75	3.49	3.09	2.6	–
h	11	11	–	–	–	–	–	–	–	–	–	–	–	–	–	–	–	–	–	–	–	–	− 0.9	− 1.39	− 1.86	− 2.34	-2.51	-2.3	–
g	12	0	–	–	–	–	–	–	–	–	–	–	–	–	–	–	–	–	–	–	–	–	− 2.2	− 2.15	− 2.12	− 2.09	-2.00	-2.0	–
g	12	1	–	–	–	–	–	–	–	–	–	–	–	–	–	–	–	–	–	–	–	–	− 0.3	− 0.29	− 0.21	− 0.16	-0.13	-0.1	–
h	12	1	–	–	–	–	–	–	–	–	–	–	–	–	–	–	–	–	–	–	–	–	− 0.4	− 0.55	− 0.87	− 1.08	-1.15	-1.2	–
g	12	2	–	–	–	–	–	–	–	–	–	–	–	–	–	–	–	–	–	–	–	–	0.2	0.21	0.30	0.46	0.43	0.4	–
h	12	2	–	–	–	–	–	–	–	–	–	–	–	–	–	–	–	–	–	–	–	–	0.3	0.23	0.27	0.37	0.52	0.6	–
g	12	3	–	–	–	–	–	–	–	–	–	–	–	–	–	–	–	–	–	–	–	–	0.9	0.89	1.04	1.23	1.28	1.2	–
h	12	3	–	–	–	–	–	–	–	–	–	–	–	–	–	–	–	–	–	–	–	–	2.5	2.38	2.13	1.75	1.37	1.0	–
g	12	4	–	–	–	–	–	–	–	–	–	–	–	–	–	–	–	–	–	–	–	–	− 0.2	− 0.38	− 0.63	− 0.89	− 1.14	− 1.2	–
h	12	4	–	–	–	–	–	–	–	–	–	–	–	–	–	–	–	–	–	–	–	–	− 2.6	− 2.63	− 2.49	− 2.19	− 1.81	− 1.5	–
g	12	5	–	–	–	–	–	–	–	–	–	–	–	–	–	–	–	–	–	–	–	–	0.9	0.96	0.95	0.85	0.71	0.6	–
h	12	5	–	–	–	–	–	–	–	–	–	–	–	–	–	–	–	–	–	–	–	–	0.7	0.61	0.49	0.27	0.08	0.0	–
g	12	6	–	–	–	–	–	–	–	–	–	–	–	–	–	–	–	–	–	–	–	–	− 0.5	− 0.30	− 0.11	0.1	0.31	0.5	–
h	12	6	–	–	–	–	–	–	–	–	–	–	–	–	–	–	–	–	–	–	–	–	0.3	0.40	0.59	0.72	0.71	0.6	–
g	12	7	–	–	–	–	–	–	–	–	–	–	–	–	–	–	–	–	–	–	–	–	0.3	0.46	0.52	0.54	0.49	0.5	–
h	12	7	–	–	–	–	–	–	–	–	–	–	–	–	–	–	–	–	–	–	–	–	0.0	0.01	0.00	− 0.09	− 0.15	− 0.2	–
g	12	8	–	–	–	–	–	–	–	–	–	–	–	–	–	–	–	–	–	–	–	–	− 0.3	− 0.35	− 0.39	− 0.37	− 0.26	− 0.1	–
h	12	8	–	–	–	–	–	–	–	–	–	–	–	–	–	–	–	–	–	–	–	–	0.0	0.02	0.13	0.29	0.55	0.8	–
g	12	9	–	–	–	–	–	–	–	–	–	–	–	–	–	–	–	–	–	–	–	–	− 0.4	− 0.36	− 0.37	− 0.43	− 0.47	− 0.5	–
h	12	9	–	–	–	–	–	–	–	–	–	–	–	–	–	–	–	–	–	–	–	–	0.3	0.28	0.27	0.23	0.16	0.1	–
g	12	10	–	–	–	–	–	–	–	–	–	–	–	–	–	–	–	–	–	–	–	–	− 0.1	0.08	0.21	0.22	0.09	− 0.2	–
h	12	10	–	–	–	–	–	–	–	–	–	–	–	–	–	–	–	–	–	–	–	–	− 0.9	− 0.87	− 0.86	− 0.89	− 0.93	-0.9	–
g	12	11	–	–	–	–	–	–	–	–	–	–	–	–	–	–	–	–	–	–	–	–	− 0.2	− 0.49	− 0.77	− 0.94	− 1.13	-1.2	–
h	12	11	–	–	–	–	–	–	–	–	–	–	–	–	–	–	–	–	–	–	–	–	− 0.4	− 0.34	− 0.23	− 0.16	− 0.04	0.1	–
g	12	12	–	–	–	–	–	–	–	–	–	–	–	–	–	–	–	–	–	–	–	–	− 0.4	− 0.08	0.04	− 0.03	− 0.33	− 0.7	–

Table 2 (continued)

	deg	ord	IGRF	IGRF	IGRF	IGRF	IGRF	IGRF	IGRF	IGRF	IGRF	DGRF	DGRF	DGRF	DGRF	DGRF	DGRF	DGRF	DGRF	DGRF	DGRF	DGRF	DGRF	DGRF	DGRF	DGRF	IGRF	SV	
h	12	12	–	–	–	–	–	–	–	–	–	–	–	–	–	–	–	–	–	–	–	–	0.8	0.88	0.87	0.72	0.52	0.2	–
g	13	0	–	–	–	–	–	–	–	–	–	–	–	–	–	–	–	–	–	–	–	–	− 0.2	− 0.16	− 0.09	− 0.02	0.08	0.2	–
g	13	1	–	–	–	–	–	–	–	–	–	–	–	–	–	–	–	–	–	–	–	–	− 0.9	− 0.88	− 0.89	− 0.92	− 0.93	− 0.9	–
h	13	1	–	–	–	–	–	–	–	–	–	–	–	–	–	–	–	–	–	–	–	–	− 0.9	− 0.76	− 0.87	− 0.88	− 0.88	− 0.9	–
g	13	2	–	–	–	–	–	–	–	–	–	–	–	–	–	–	–	–	–	–	–	–	0.3	0.30	0.31	0.42	0.53	0.6	–
h	13	2	–	–	–	–	–	–	–	–	–	–	–	–	–	–	–	–	–	–	–	–	0.2	0.33	0.30	0.49	0.64	0.7	–
g	13	3	–	–	–	–	–	–	–	–	–	–	–	–	–	–	–	–	–	–	–	–	0.1	0.28	0.42	0.63	0.72	0.7	–
h	13	3	–	–	–	–	–	–	–	–	–	–	–	–	–	–	–	–	–	–	–	–	1.8	1.72	1.66	1.56	1.40	1.2	–
g	13	4	–	–	–	–	–	–	–	–	–	–	–	–	–	–	–	–	–	–	–	–	− 0.4	− 0.43	− 0.45	− 0.42	− 0.30	− 0.2	–
h	13	4	–	–	–	–	–	–	–	–	–	–	–	–	–	–	–	–	–	–	–	–	− 0.4	− 0.54	− 0.59	− 0.5	− 0.38	− 0.3	–
g	13	5	–	–	–	–	–	–	–	–	–	–	–	–	–	–	–	–	–	–	–	–	1.3	1.18	1.08	0.96	0.75	0.5	–
h	13	5	–	–	–	–	–	–	–	–	–	–	–	–	–	–	–	–	–	–	–	–	− 1.0	− 1.07	− 1.14	− 1.24	− 1.31	− 1.3	–
g	13	6	–	–	–	–	–	–	–	–	–	–	–	–	–	–	–	–	–	–	–	–	− 0.4	− 0.37	− 0.31	− 0.19	− 0.01	0.1	–
h	13	6	–	–	–	–	–	–	–	–	–	–	–	–	–	–	–	–	–	–	–	–	− 0.1	− 0.04	− 0.07	− 0.1	− 0.09	− 0.1	–
g	13	7	–	–	–	–	–	–	–	–	–	–	–	–	–	–	–	–	–	–	–	–	0.7	0.75	0.78	0.81	0.76	0.7	–
h	13	7	–	–	–	–	–	–	–	–	–	–	–	–	–	–	–	–	–	–	–	–	0.7	0.63	0.54	0.42	0.29	0.2	–
g	13	8	–	–	–	–	–	–	–	–	–	–	–	–	–	–	–	–	–	–	–	–	− 0.4	− 0.26	− 0.18	− 0.13	− 0.05	0.0	–
h	13	8	–	–	–	–	–	–	–	–	–	–	–	–	–	–	–	–	–	–	–	–	0.3	0.21	0.10	− 0.04	− 0.11	− 0.2	–
g	13	9	–	–	–	–	–	–	–	–	–	–	–	–	–	–	–	–	–	–	–	–	0.3	0.35	0.38	0.38	0.37	0.3	–
h	13	9	–	–	–	–	–	–	–	–	–	–	–	–	–	–	–	–	–	–	–	–	0.6	0.53	0.49	0.48	0.47	0.5	–
g	13	10	–	–	–	–	–	–	–	–	–	–	–	–	–	–	–	–	–	–	–	–	− 0.1	− 0.05	0.02	0.08	0.13	0.2	–
h	13	10	–	–	–	–	–	–	–	–	–	–	–	–	–	–	–	–	–	–	–	–	0.3	0.38	0.44	0.48	0.54	0.6	–
g	13	11	–	–	–	–	–	–	–	–	–	–	–	–	–	–	–	–	–	–	–	–	0.4	0.41	0.42	0.46	0.45	0.4	–
h	13	11	–	–	–	–	–	–	–	–	–	–	–	–	–	–	–	–	–	–	–	–	− 0.2	− 0.22	− 0.25	− 0.3	− 0.41	− 0.6	–
g	13	12	–	–	–	–	–	–	–	–	–	–	–	–	–	–	–	–	–	–	–	–	0.0	− 0.10	− 0.26	− 0.35	− 0.46	− 0.5	–
h	13	12	–	–	–	–	–	–	–	–	–	–	–	–	–	–	–	–	–	–	–	–	− 0.5	− 0.57	− 0.53	− 0.43	− 0.36	− 0.3	–
g	13	13	–	–	–	–	–	–	–	–	–	–	–	–	–	–	–	–	–	–	–	–	0.1	− 0.18	− 0.26	− 0.36	− 0.40	− 0.4	–
h	13	13	–	–	–	–	–	–	–	–	–	–	–	–	–	–	–	–	–	–	–	–	− 0.9	− 0.82	− 0.79	− 0.71	− 0.60	− 0.5	–

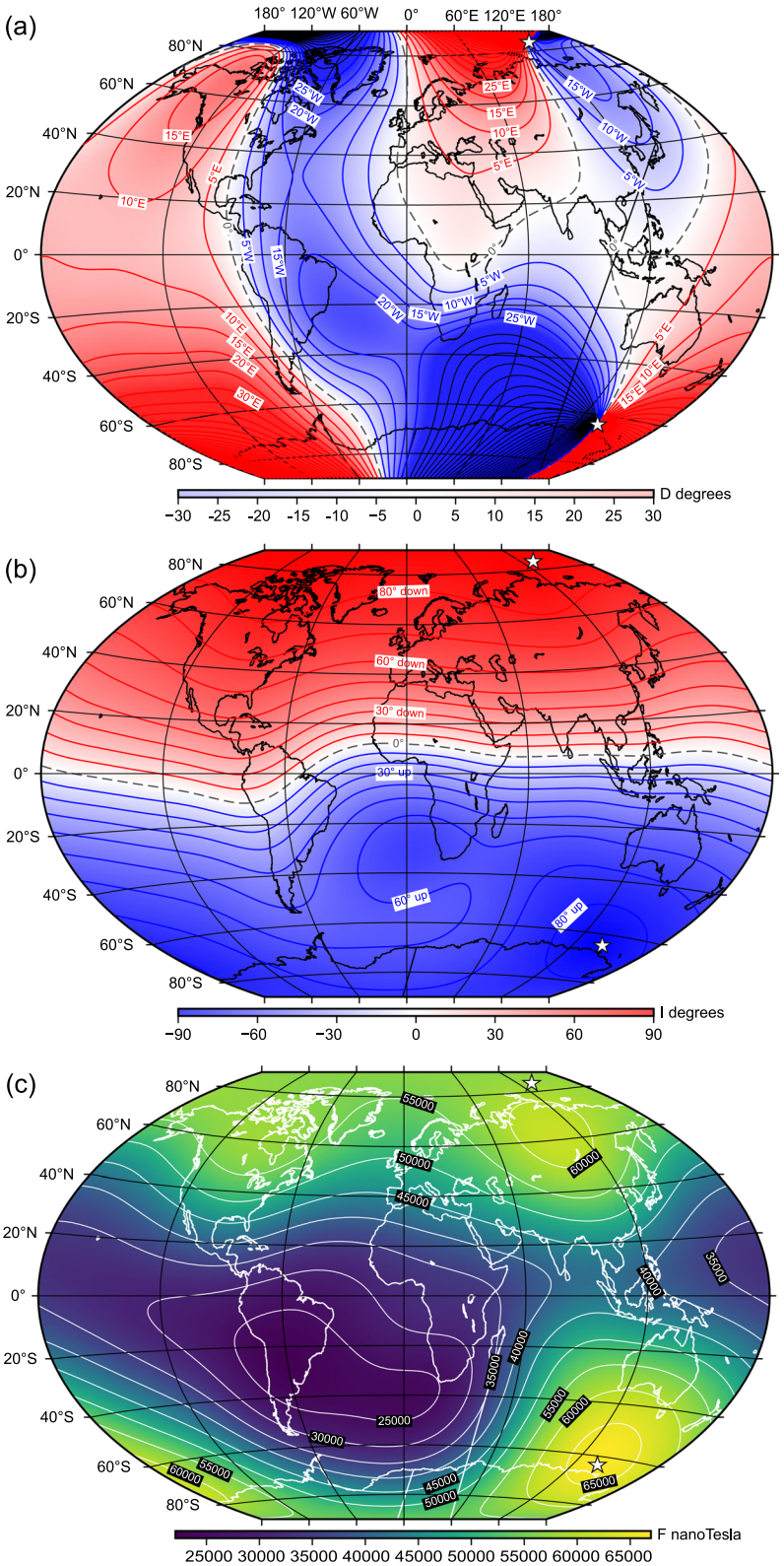

Fig. 1 Maps of (**a**) declination and (**b**) inclination angle and (**c**) total field intensity at the WGS-84 ellipsoid surface for epoch 2025.0. For (**a**) and (**b**) the zero contour is shown as a dashed black line, positive contours in red, and negative contours in blue. White stars indicate the approximate locations of the north and south magnetic dip poles. Projection is Winkel Tripel

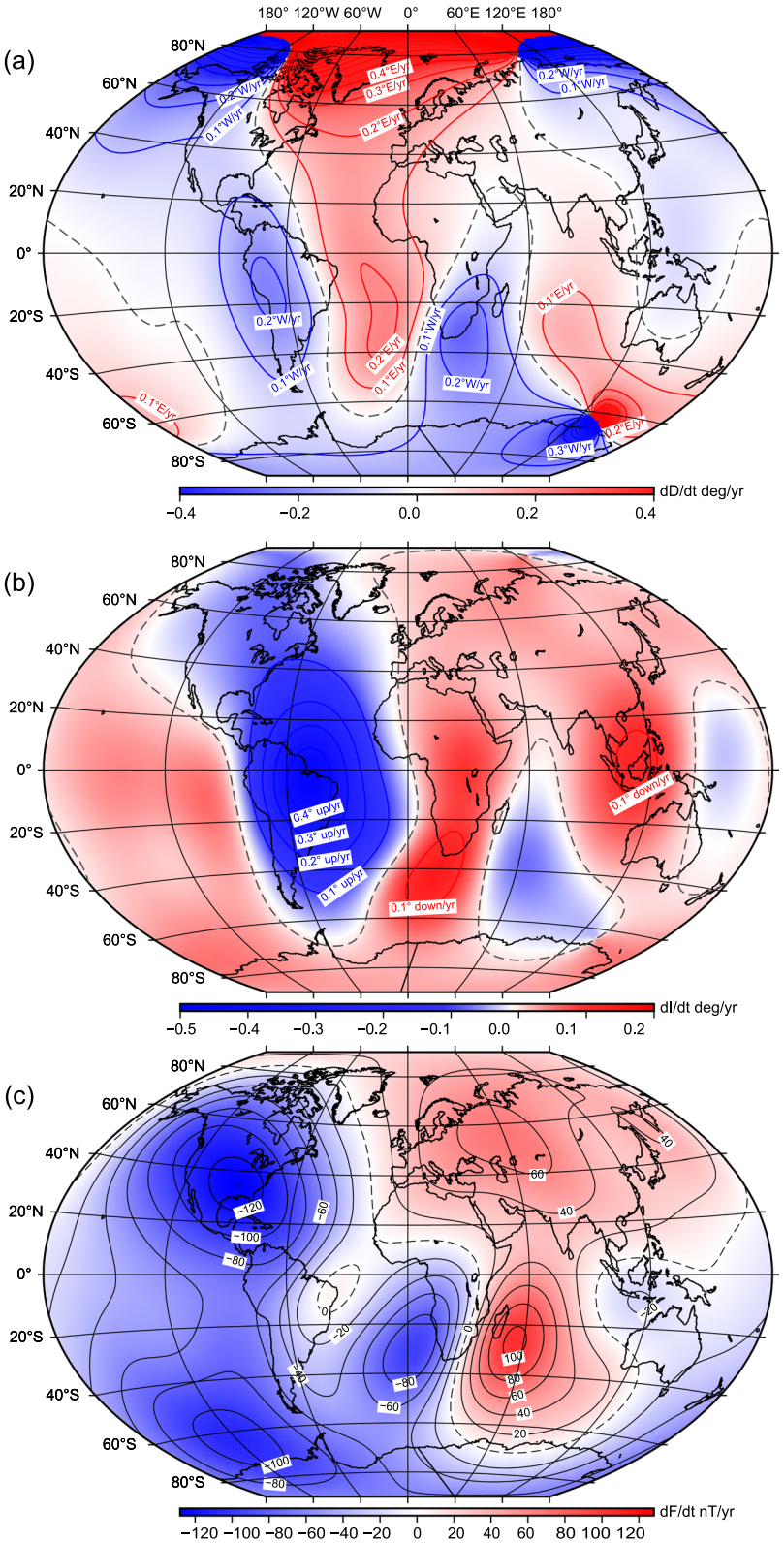

Fig. 2 Maps of predicted annual secular variation in (**a**) declination, (**b**) inclination and (**c**) total field at the WGS-84 ellipsoid surface averaged over 2025–2030. The zero contour is shown as the dashed black line, positive contours in red, and negative contours in blue. Projection is Winkel Tripel

Absolute Scalar Magnetometer instrument (Hulot et al. 2015; Léger et al. 2015) as well as data from the Ørsted (Olsen 2007), CHAMP (Maus 2007), SAC-C (Colomb et al. 2004), Cryosat-2 (Olsen et al. 2020), and CSES (Shen et al. 2018) missions were also used by some of the teams. For the first time, data from the Macau Science Satellite 1 (MSS-1) (Zhang 2023; Jiang et al. 2024) were included in several IGRF candidates.

The IGRF-14 Evaluation Taskforce voted to calculate the final main field model for epoch 2020.0 as the median of the Gauss coefficients of all the candidate models. The task force voted to use a robust Huber weighting in space to determine the final coefficients for the 2025 main field epoch and for the secular variation model for 2025.0–2030.0. Further details of the candidate models, the evaluation process, and the final model determination are provided in Beggan et al. (2026).

4 IGRF-14 model coefficients and maps

Table 2 lists the IGRF-14 spherical harmonic Gauss coefficients, which can be used with Eq. (1) to determine the geomagnetic potential (and vector geomagnetic field) anywhere on or above Earth's surface. This table serves as a published record of IGRF-14, which should allow users to ensure they use the correct model coefficients for a particular epoch compared with previous generations. The main field coefficients are given in units of nT, and the predictive secular variation coefficients (last column) are given in units of nT/year. These coefficients are available in digital form from https://www.ncei.noaa.gov/products/international-geomagnetic-reference-field along with software to compute magnetic field components at different times and spatial locations, in both geocentric and geodetic coordinate systems.

A new innovation in IGRF-14 has been to establish an open access record of the candidates and final coefficient

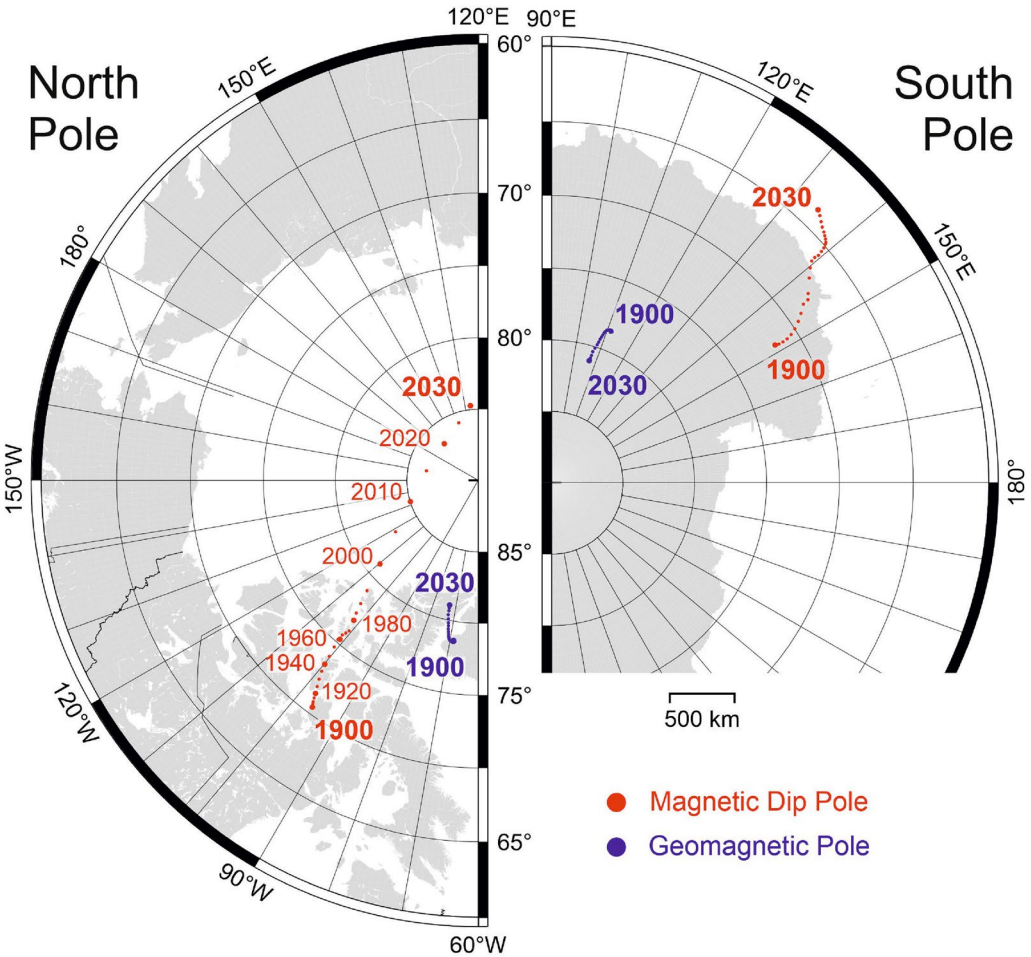

Fig. 3 Motion of the magnetic dip pole (red) and geomagnetic pole (blue) since 1900 from IGRF-14 in the northern hemisphere (left) and southern hemisphere (right). The scale provides an indication of distance on the WGS-84 ellipsoid that is correct along lines of constant longitude and also along the middle lines of latitude shown. Note the left and right panels use different longitude ranges. The maps use stereographic projection

files in a GitHub repository (Beggan et al. 2024) and to deposit the final coefficients in a Zenodo repository (International Association of Geomagnetism and Aeronomy (2024)). These make finding and reproducing the IGRF-14 coefficients compliant with FAIR standards (e.g., Ayala et al. 2022).

Using Equation 1 allows the North (X), East (Y) and Vertical (Z) components of the magnetic field vector to be computed. These three orthogonal components can be converted to the angles more familiar to compass users of Declination (D) and Inclination (I), along with the Total Field intensity (F). Taken together, these three quantities fully describe the vector magnetic field at Earth's surface:

$$D = \tan^{-1}(Y/X), \tag{6}$$

$$I = \tan^{-1}\left(Z/\sqrt{X^2+Y^2}\right), \tag{7}$$

$$F = \sqrt{X^2+Y^2+Z^2}. \tag{8}$$

In the convention of geomagnetism, a deviation of the compass needle west of True North is considered to be negative Declination while east of True North is positive. A needle with its north magnetic pole pointing into the ground is considered to have positive Inclination while negative Inclination is when the north pole of the needle points upward away from the ground. Compasses generally have positive Inclination in the northern hemisphere and negative in the south, though this is not true everywhere. The total field is a scalar value which is always positive and varies between 22,000 nT and 70,000 nT on the Earth's surface.

The IGRF-14 provides magnetic values in geocentric spherical coordinates which must be converted to geodetic coordinates using a reference ellipsoid, usually WGS-84. This involves computing the equivalent geodetic latitude and rotating the X and Z magnetic components to compensate for the change in the normal vector.

Figure 1 shows global maps of the geodetic IGRF-14 declination (D), inclination (I), and total field intensity (F) on Earth's surface in 2025.0 in Winkel Tripel projection. For the declination component (top panel), the dashed lines are the agonic lines (zero declination angle) on which a magnetic compass needle points to true geographic north. For the inclination map (middle panel), the dashed contour line of zero inclination angle and is known as the magnetic dip equator. It approximately aligns with the geographic equator except for a large, well-known southward deviation over South America. The total field (F) map (bottom panel) shows that the highest field intensities occur in Siberia in the northern hemisphere and in the Southern Ocean between Australia and Antarctica in the southern hemisphere. We also see a region of significantly weaker field (compared to an idealized dipole), centered over South America, which is known as the South Atlantic Anomaly. The South Atlantic Anomaly has deepened by around 150 nT over the last five years and moved westward at around 20 km/year. The minimum total field value at 2025.0 on the Earth's surface is 22,071 nT and lies at 26.22°S, 60.03°W in a rural area of northeastern Argentina. We

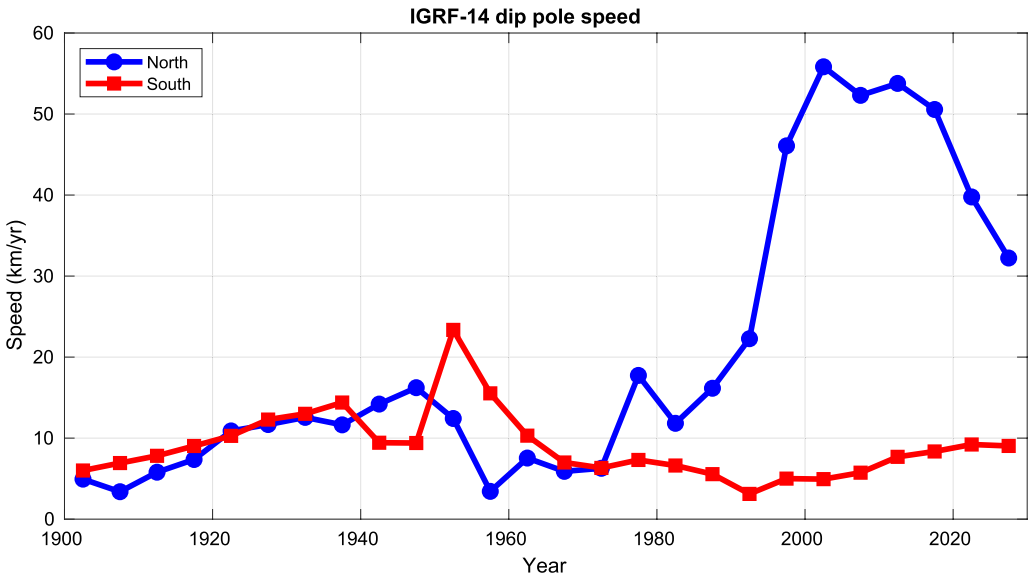

Fig. 4 Average speed of the magnetic dip poles over each five year epoch, plotted at the midpoint between epochs (i.e. the speed over 2020–2025 is shown at 2022.5). The value for 2025–2030 is a forecast

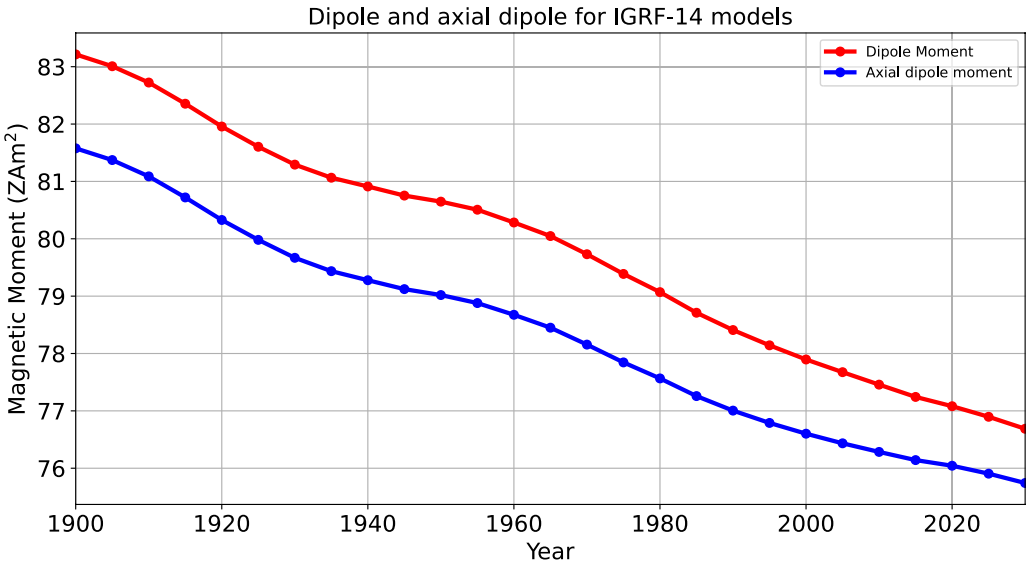

Fig. 5 Dipole and axial dipole moment time series derived from IGRF-14 in units of Zetta (10^{21}) Am^2. The value for 2030 is a forecast

Table 3 Magnetic pole position since 1900 determined from IGRF-14 in units of degrees

	North dip pole		South dip pole		North geomagnetic pole		South geomagnetic pole	
Epoch	**Latitude**	**Longitude**	**Latitude**	**Longitude**	**Latitude**	**Longitude**	**Latitude**	**Longitude**
1900.0	70.46	− 96.19	− 71.72	148.32	78.68	− 68.79	− 78.68	111.21
1905.0	70.66	− 96.48	− 71.46	148.54	78.68	− 68.75	− 78.68	111.25
1910.0	70.79	− 96.72	− 71.15	148.64	78.66	− 68.72	− 78.66	111.28
1915.0	71.03	− 97.03	− 70.80	148.54	78.64	− 68.57	− 78.64	111.43
1920.0	71.34	− 97.38	− 70.41	148.20	78.63	− 68.38	− 78.63	111.62
1925.0	71.79	− 97.99	− 69.99	147.62	78.62	− 68.27	− 78.62	111.73
1930.0	72.27	− 98.68	− 69.52	146.79	78.60	− 68.26	− 78.60	111.74
1935.0	72.80	− 99.33	− 69.06	145.76	78.57	− 68.36	− 78.57	111.64
1940.0	73.30	− 99.87	− 68.57	144.59	78.55	− 68.51	− 78.55	111.49
1945.0	73.93	− 100.24	− 68.15	144.44	78.55	− 68.53	− 78.55	111.47
1950.0	74.64	− 100.86	− 67.89	143.55	78.55	− 68.85	− 78.55	111.15
1955.0	75.18	− 101.42	− 67.19	141.50	78.54	− 69.16	− 78.54	110.84
1960.0	75.30	− 101.03	− 66.70	140.23	78.58	− 69.47	− 78.58	110.53
1965.0	75.63	− 101.34	− 66.33	139.53	78.60	− 69.85	− 78.60	110.15
1970.0	75.88	− 100.97	− 66.02	139.40	78.66	− 70.18	− 78.66	109.82
1975.0	76.15	− 100.64	− 65.74	139.52	78.76	− 70.47	− 78.76	109.53
1980.0	76.91	− 101.68	− 65.42	139.35	78.88	− 70.76	− 78.88	109.24
1985.0	77.40	− 102.61	− 65.13	139.18	79.04	− 70.90	− 79.04	109.10
1990.0	78.10	− 103.69	− 64.91	138.90	79.21	− 71.13	− 79.21	108.87
1995.0	79.04	− 105.29	− 64.79	138.73	79.39	− 71.42	− 79.39	108.58
2000.0	80.97	− 109.64	− 64.66	138.30	79.61	− 71.57	− 79.61	108.43
2005.0	83.19	− 118.22	− 64.55	137.85	79.82	− 71.81	− 79.82	108.19
2010.0	85.02	− 132.84	− 64.43	137.32	80.09	− 72.21	− 80.09	107.79
2015.0	86.31	− 160.34	− 64.28	136.60	80.38	− 72.61	− 80.38	107.39
2020.0	86.49	162.80	− 64.08	135.87	80.65	− 72.68	− 80.65	107.32
2025.0	85.73	138.65	− 63.86	135.07	80.85	− 72.76	− 80.85	107.24
2030.0	84.73	125.94	− 63.66	134.27	81.05	− 72.96	− 81.05	107.04

Latitudes are provided in the WGS-84 geodetic system

Table 4 Magnetic observatories contributing data used in the construction of IGRF-14.

Supporting agencies	Country	Observatory IAGA code
Centre de Recherche en Astronomie, Astrophysique et Geophysique	Algeria	TAM
Universidad Nacional de la Plata	Argentina	TRW
Servicio Meteorologico Nacional	Argentina	PIL, ORC
Geoscience Australia	Australia	ASP, CKI, CNB, CSY, CTA, DVS
		GNA, GNG, KDU, LRM, MAW, MCQ
Geosphere Austria	Austria	WIC
Institut Royal Météorologique	Belgium	DOU, MAB
CNPq-Observatorio Nacional	Brazil	VSS, TTB
Bulgarian Academy of Sciences	Bulgaria	PAG
Geological Survey of Canada	Canada	ALE, BLC, BRD, CBB, FCC, IQA
		MEA, OTT, RES, STJ, VIC,YKC
Dirección Meteorológica de Chile	Chile	IPM
Academy of Sciences	China	BMT, SSH
China Earthquake Administration	China	CDP, CNH, GLM, GZH, KSH, LZH
		MZL, QGZ, QIX, QZH, THJ, WHN
Instituto Geographico Agustin Codazzi	Columbia	FUQ
University of Zagreb	Croatia	LON
Academy of Sciences of the Czech Republic	Czechia	BDV
Technical University of Denmark, DTU Space	Denmark	BFE, NAQ, GDH, THL
Addis Ababa University	Ethiopia	AAE
Finnish Meteorological Institute	Finland	NUR
Geophysical Observatory	Finland	SOD
Institut de Physique du Globe de Paris	France	AAE, BOX, CLF, DLT, KOU, IPM
		LZH, MBO, PHU, PPT, TAM
Ecole et Observatoire des Sciences de la Terre	France	AMS, CZT, DMC, DRV, PAF, TAN
Universität München	Germany	FUR
Alfred-Wegener-Institute for Polar Marine Research	Germany	VNA
GFZ Helmholtz Centre for Geosciences	Germany	ABG, BFO, GAN, KMH, LRV, NGK, PAG, SHE,
		SUA, STT, TDC, TTB, VNA, VSS, WNG
Universität Stuttgart and KIT	Germany	BFO
Institute of Geology and Mineral Exploration	Greece	PEG
Academy of Sciences	Hungary	NCK
Mining and Geological Survey of Hungary	Hungary	THY
University of Iceland	Iceland	LRV
Indian Institute of Geomagnetism	India	ABG, JAI, NGP, PND, SIL
		SHL, TIR, UJJ, VSK
National Geophysical Research Institute	India	CPL, HYB
Meteorological and Geophysical Agency	Indonesia	KPG, PLR, TND, TUN
Met Éireann	Ireland	VAL
Survey of Israel	Israel	AMT, BGY, ELT
Instituto Nazionale di Geofisica e Vulcanologia	Italy	AQU, CTS, DMC
Japan Meteorological Agency	Japan	CBI, KAK, KNY, MMB
Geospatial Information Authority of Japan	Japan	ESA, KNZ, MIZ
Institute of the Ionosphere	Kazakhstan	AAA
Korean Meteorological Administration	Rep of Korea	CYG
Institut et Observatoire Géophysique d'Antananarivo	Madagascar	TAN
Maldives Meteorological Service	Maldives	GAN
Institute of Geological and Nuclear Sciences	New Zealand	API, EYR, SBA
University of Tromsø	Norway	BJN, DOB, TRO

Table 4 (continued)

Supporting agencies	Country	Observatory IAGA code
Instituto Geofisico del Peru	Peru	HUA
Academy of Sciences	Poland	BEL, HLP, HRN
Universidade de Coimbra	Portugal	COI
Instituto Português do Mar e da Atmosfera	Portugal	STT
Geological Survey of Romania	Romania	SUA
AARI	Russia	VOS
GC RAS	Russia	ARS, KLI, MHV, SPG
IPE RAS	Russia	BOX
IG UB RAS	Russia	ARS
IDG RAS	Russia	MHV
IKIR FEB RAS	Russia	KHB, MGD, PET
IPGG SB RAS	Russia	NVS
ISTP SB RAS	Russia	IRT
IZMIRAN SpB Branch	Russia	SPG
SHICRA SB RAS	Russia	YAK
Dept. of Agriculture, Forestry, Fisheries & Meteorology	Samoa	API
Geomagnetic College Grocka	Serbia	GCK
Slovenska Akademia Vied	Slovakia	HRB
National Research Foundation	South Africa	HBK, HER, KMH, TSU
Observatori de l'Ebre	Spain	EBR, LIV
Real Instituto y Observatorio de la Armada	Spain	SFS
Instituto Geográfico Nacional	Spain	GUI, SPT
Sveriges Geologiska Undersökning	Sweden	ABK, LYC, UPS
Swedish Institute of Space Physics	Sweden	KIR
ETH Zurich	Switzerland	GAN
Boğaziçi University	Türkiye	IZN
Academy of Sciences	Ukraine	AIA, LVV
British Geological Survey	United Kingdom	ASC, ESK, HAD, JCO, KEP, LER, PST, SBL
US Geological Survey	United States	BRW, BOU, BSL, CMO, DED, FRD, FRN GUA, HON, NEW, SIT, SJG, SHU, TUC
Institute of Geophysics of the Vietnamese Academy of Science and Technology	Vietnam	DLT, PHU

also point out that a second low point in the South Atlantic Ocean, offshore of South Africa, continues to grow as noted by Finlay et al. (2020) and Rother et al. (2021).

Figure 2 shows the predicted average change of the *D*, *I*, and *F* components on Earth's surface during the interval between 2025 and 2030. At low and middle latitudes, the map of d*D*/dt (top panel) predicts the largest declination changes in the South Atlantic Anomaly region and also in the polar regions, with northern polar declination angle changing more than in the southern polar region. The d*I*/dt map (middle panel) predicts the largest changes over Brazil, where the magnetic dip equator has moved relatively rapidly over the past few decades. The largest changes in field strength (d*F*/dt) are modeled in North America (of -128 nT/yr) while the Indian Ocean also has a variation of 104 nT/yr.

Figure 3 presents the positions of the *geomagnetic* poles and *dip* poles as given by IGRF-14 for 1900–2025, and their predicted positions in 2030. The geomagnetic poles are calculated from the three dipole ($n = 1$) Gauss coefficients and correspond to where the magnetic dipole axis intersects a sphere of mean Earth radius (6371.2 km). These poles are antipodal and are also known as centered dipole poles (Laundal and Richmond 2017, Eq. 14). The geomagnetic poles can be used to specify the relative orientation of Earth's magnetic field with respect to the Sun, and they are often used in magnetospheric studies for this purpose.

The magnetic *dip* poles are defined as the locations where the main magnetic field is normal (inclination angle is 90°) to Earth's surface, as represented by the WGS-84 reference ellipsoid. Here, we use the full set

of IGRF-14 coefficients to spherical harmonic degree and order $N = 13$. The location of the dip pole is found by searching for the position where the horizontal field component ($H = \sqrt{X^2 + Y^2}$) is zero. We use a gradient descent search algorithm to find this point on a grid of 0.01° resolution to give a modeled location to within 1 km accuracy. In reality, the influence of secular variation and the external magnetic field will cause the true location to move continuously.

Magnetic dip poles provide a key reference for local orientation when navigating on or close to Earth's surface at high-latitudes. However, note that in general a compass needle does not point to the dip pole but aligns along the local magnetic field direction. For a perfect dipole field, the geomagnetic and dip poles would nearly coincide, but not exactly since the geomagnetic poles are defined with respect to a sphere of mean Earth radius, while the dip poles are defined with respect to the WGS-84 ellipsoid. As can be seen in Figure 3, there are significant differences between the two due to the non-dipolar structure of Earth's magnetic field. The geomagnetic and dip pole locations are provided in Table 3. Interestingly, IGRF-14 predicts the magnetic north and south dip poles will briefly have the same longitude (around 136°W) in early 2026.

Figure 4 shows the speed of the two magnetic dip poles. The north magnetic dip pole experienced a strong acceleration from about 1960–2000, but has seen a modest deceleration over the past 25 years, peaking at 56 km/year in 2002.5 and slowing to 40 km/year in 2012.5. IGRF-14 forecasts continued deceleration with a speed of 31 km/year in 2027.5. This equates to a dip pole motion of about 100 m/day. However, past IGRF forecasts have often over- or underestimated the dip pole velocity (Finlay et al. 2010b). As with any model, uncertainties are present in IGRF and are further discussed by Lowes (2000).

Using the ratio of the dipole to non-dipole terms from the Lowes–Mauersberger power spectrum (Beggan et al. 2026) at Earth's surface in 2025, the contribution from the dipole terms g_1^0, g_1^1, h_1^1 account for 92.31% of the power in the main geomagnetic field, a slight fall from 92.52% in 2020. Figure 5 shows the decline in the dipole moment of the geomagnetic field since 1900 as predicted by IGRF-14 (red). The dipole moment is defined as:

$$M(t) = \frac{4\pi}{\mu_0} a^3 \sqrt{g_1^0(t)^2 + g_1^1(t)^2 + h_1^1(t)^2}, \quad (9)$$

where μ_0 is the permeability of free space ($4\pi \times 10^{-7}$ H/m). Archaeomagnetic and palaeomagnetic studies often estimate the dipole strength along the rotation axis, ignoring the off-axis terms g_1^1, h_1^1. This axial dipole moment is defined as $M_A(t) = 4\pi a^3 |g_1^0(t)|/\mu_0$ and is consequently lower, as shown in blue in the figure. The dipole field is forecast to continue to fall in strength over the next five years and weaken relative to the non-dipolar contributions.

5 Conclusion

We present the 14th generation of the International Geomagnetic Reference Field. The model is valid from 1900.0 to 2030.0, describing the internal magnetic field of the Earth using spherical harmonic Gauss coefficients to degree and order 13 with snapshots every five years. The final snapshot between 2025.0 and 2030.0 is a forecast of secular variation to degree and order 8.

The IGRF is a truly international effort involving thousands of observers, scientists and engineers from around the world. Without their contributions, this would not be possible. This generation introduced the use of open source software tools including data repositories and automated evaluation code. The IGRF-14 coefficients, model code and maps are freely available for use. They can be found both within and at the online sources noted in this paper.

6 IGRF-14 online data products

Coefficients of IGRF-14 in ASCII format, other data formats, programs, software and further general information about IGRF:

https://www.ncei.noaa.gov/products/international-geomagnetic-reference-field

Coefficients of IGRF-14 (Zenodo repository): https://doi.org/10.5281/zenodo.14218973

IGRF-14 candidate models and evaluation code (GitHub repository): https://github.com/IAGA-VMOD/IGRF14eval

Python software to compute magnetic field components from coefficients (Laundal et al. 2024): https://doi.org/10.5281/zenodo.14231854

Online calculation of magnetic field components for IGRF-14:

https://www.ncei.noaa.gov/products/international-geomagnetic-reference-field

http://geomag.bgs.ac.uk/data_service/models_compass/igrf_calc.html

http://wdc.kugi.kyoto-u.ac.jp/igrf/point/index.html

World Data System

WORLD DATA SERVICE FOR GEOPHYSICS, BOULDER

NOAA National Centers for Environmental Information

325 Broadway, E/NE42, Boulder, CO, 80305-3328, UNITED STATES OF AMERICA

TEL: +1 828 271 4800

EMAIL: ncei.info@noaa.gov

INTERNET: https://www.ncei.noaa.gov/services/world-data-system

WORLD DATA CENTER FOR GEOMAGNETISM, COPENHAGEN

Technical University of Denmark, DTU Space, Centrifugevej, Building 356, DK 2800, Kgs. Lyngby, DENMARK

TEL: +45 4525 9713

EMAIL: anna@space.dtu.dk

INTERNET: https://www.space.dtu.dk/english/research/scientific_data_and_models

WORLD DATA CENTRE FOR GEOMAGNETISM, EDINBURGH

British Geological Survey

The Lyell Centre

Edinburgh, EH14 4AP

UNITED KINGDOM

TEL: +44 131 667 1000

EMAIL: wdcgeomag@bgs.ac.uk

INTERNET: https://wdc.bgs.ac.uk

WORLD DATA CENTER FOR GEOMAGNETISM, KYOTO

Data Analysis Center for Geomagnetism and Space Magnetism

Graduate School of Science, Kyoto University

Kitashirakawa-Oiwake Cho, Sakyo-ku

Kyoto, 606-8502, JAPAN

TEL: +81 75 753 3929

FAX: +81 75 722 7884

EMAIL: toh@kugi.kyoto-u.ac.jp

INTERNET: https://wdc.kugi.kyoto-u.ac.jp/

WORLD DATA CENTER FOR SOLID EARTH PHYSICS, MOSCOW

Geophysical Center of the Russian Academy of Sciences

Molodezhnaya, 3

Moscow, 119296, RUSSIA

TEL: +7 495 930 56 49

EMAIL: wdcsep@wdcb.ru

INTERNET: http://www.wdcb.ru/sep/index.html

WORLD DATA CENTRE FOR GEOMAGNETISM, MUMBAI

Indian Institute of Geomagnetism

New Panvel(W), Navi Mumbai, 410 218, INDIA

TEL: +91-22-2748 4000

EMAIL: iig.postmast@iigm.res.in

INTERNET: https://iigm.res.in/facilities-service-corners/world-data-centre

Acknowledgements

We acknowledge the indirect contributions from the many scientists, support staff, engineers and observers who support magnetic measurements and research. The European Space Agency (ESA) is gratefully acknowledged for providing access to the Swarm magnetic field data and for making it possible for IPGP and CEA-Léti to derive the additional ASM-V experimental data from the CNES-funded ASM instrument, all used in this work. The China National Space Administration and the China Earthquake Administration are acknowledged for providing access to CSES magnetometer data. This work utilized the scientific data from the Macau Science Satellite-1, owned by China National Space Administration and the Macau SAR Government. The results presented in this paper rely on data collected at magnetic observatories. We thank the national institutes that support them and INTERMAGNET for promoting high standards of magnetic observatory practice (https://www.intermagnet.org). We acknowledge the continued support of IAGA for the production of the IGRF. This paper is published with the permission of the Executive Director of the British Geological Survey (UKRI).

Author contributions

C.D. Beggan is chair of the IAGA DIV V-MOD (2023-2027) and initiated, coordinated and organized the call and delivery of the 14th generation of the IGRF. C. Kloss is co-chair (2023-2027). CDB and CK wrote the manuscript based on the analyses of the contributing co-authors. All other authors contributed modelling results and/or detailed technical analyses for IGRF-14. All co-authors have read and approved the manuscript.

Funding

The Swarm and Cryosat-2 missions are owned and operated by the European Space Agency (ESA). The Ørsted mission was made possible by extensive support from the Danish government, NASA, ESA, CNES, DARA, and the Thomas B. Thriges Foundation. The CHAMP mission was sponsored by the Space Agency of the German Aerospace Center (DLR) through funds of the Federal Ministry of Economics and Technology, following a decision of the German Federal Parliament (grant code 50EE0944). The SAC-C mission was made possible by a collaboration between the Comisión Nacional de Actividades Espaciales (CONAE), NASA/JPL, and the Danish Space Research Institute. The CSES mission is funded by the China National Space Administration (CNSA) and the China Earthquake Administration (CEA). The MSS-1 mission is funded by the China National Space Administration (CNSA) and the Macau Foundation. The international network of geomagnetic observatories is supported by numerous institutes, staff, and INTERMAGNET. The French contribution to this work was supported by the French Centre National des Etudes Spatiales (CNES) in the framework of the program "Exploitation de la mission satellitaire européenne Swarm." Work has been funded by the European Research Council (ERC) under the European Union's Horizon 2020 research and innovation programme (GRACEFUL Synergy Grant agreement No 855677). Work has been funded by the ESA in the framework of EO Science for Society, through contract 4000127193/19/NL/IA (Swarm +4D Deep Earth: Core). This research was supported in part by the NOAA cooperative agreement NA22OAR4320151. The statements, findings, conclusions, and recommendations are those of the author(s) and do not necessarily reflect the views of NOAA or the U.S. Department of Commerce. The Russian contribution was conducted in the framework of budgetary funding of the Geophysical Center of RAS and the Schmidt Institute of Physics of the Earth of RAS, adopted by the Ministry of Science and Higher Education of the Russian Federation.

Data availability

Swarm and Cryosat-2 data are available from https://earth.esa.int/web/guest/swarm/data-access. Swarm ASM-V experimental data are available from https://dataverse.ipgp.fr/dataverse/swarm-data. CHAMP data can be obtained from http://isdc.gfz.de. Ørsted and SAC-C data are available from https://www.space.dtu.dk/english/research/scientific_data_and_models/magnetic-satellites. CSES data are available from http://www.leos.ac.cn. Macau Science

Satellite data are available from https://mss.must.edu.mo/. INTERMAGNET data are available from https://www.intermagnet.org.

Declarations

Competing interests

The authors declare that they have no competing interests.

Author details

[1]British Geological Survey, Lyell Centre, Research Avenue South, Edinburgh EH14 4AP, UK. [2]Division of Geomagnetism and Geospace, DTU Space, Technical University of Denmark, Centrifugevej 356, 2800 Kongens Lyngby, Denmark. [3]CNRS, Univ. Grenoble Alpes, Grenoble INP, GIPSA-Lab, Grenoble, Grenoble, France. [4]University of Science and Technology Houari Boumediene, Bab-Ezzouar, Algeria. [5]Nantes Université, Univ Angers, Le Mans Université, CNRS, Laboratoire de Planétologie et Géosciences, LPG UMR 6112, Nantes, France. [6]Université Paris Cité, Institut de physique du globe de Paris, CNRS, Paris, France. [7]Technical University of Berlin, Berlin, Germany. [8]Cooperative Institute for Research in Environmental Sciences, University of Colorado Boulder, Boulder, Colorado, USA. [9]NOAA National Centers for Environmental Information, Boulder, USA. [10]Universidad Complutense de Madrid, Madrid, Spain. [11]Instituto de Geociencias IGEO, Madrid, Spain. [12]Univ. Grenoble Alpes, Univ. Savoie Mont Blanc, CNRS, IRD, Univ. Gustave Eiffel, ISTerre, Grenoble, France. [13]GFZ Helmholtz Centre for Geosciences, Potsdam, Germany. [14]School of Earth and Environment, University of Leeds, Leeds, UK. [15]Geophysical Center of the Russian Academy of Sciences (GC RAS), Moscow, Russia. [16]Laboratoire Magmas et Volcans, CNRS, IRD, OPGC, Université Clermont Auvergne, Clermont-Ferrand, France. [17]University of Cologne, Cologne, Germany. [18]NASA Goddard Space Flight Center, Greenbelt, MD, USA. [19]School of Environmental Sciences, University of Liverpool, Liverpool, UK. [20]University of Potsdam, Potsdam, Germany. [21]CEA-Leti, Université Grenoble Alpes, MINATEC, Grenoble, France. [22]Macau Institute of Space Technology and Application, Macau University of Science and Technology, Macau SAR, Macau, China. [23]School of GeoSciences, University of Edinburgh, Edinburgh, UK. [24]Centre National d'Etudes Spatiales, Paris, France. [25]Institute of Science Tokyo, Tokyo, Japan. [26]Kobe University, Kobe, Japan. [27]Institute of Statistical Mathematics, Tachikawa, Japan. [28]SHOM, Brest, France. [29]Wuhan University, Wuhan, China. [30]Kyoto University, Kyoto, Japan. [31]Schmidt Institute of Physics of the Earth of the Russian Academy of Sciences (IPE RAS), Moscow, Russia. [32]National Institute of Natural Hazards, the Ministry of Emergency Management, Beijing, China. [33]University of Strasbourg, Strasbourg, France.

Received: 14 October 2025 Accepted: 21 December 2025
Published online: 29 June 2026

References

Alken P, Thébault E, Beggan CD, Aubert J, Baerenzung J, Brown W, Califf S, Chulliat A, Cox G, Finlay CC, Fournier A, Gillet N, Hammer MD, Holschneider M, Hulot G, Korte M, Lesur V, Livermore P, Lowes F, Macmillan S, Nair M, Olsen N, Ropp G, Rother M, Schnepf NR, Stolle C, Toh H, Vervelidou F, Vigneron P, Wardinski I (2021) Evaluation of candidate models for the 13th generation International Geomagnetic Reference Field. Earth Planets Space 73:48. https://doi.org/10.1186/s40623-020-01281-4

Alken P, Thébault E, Beggan CD, Amit H, Aubert J, Baerenzung J, Bondar TN, Brown WJ, Califf S, Chambodut A, Chulliat A, Cox GA, Finlay CC, Fournier A, Gillet N, Grayver A, Hammer MD, Holschneider M, Huder L, Hulot G, Jager T, Kloss C, Korte M, Kuang W, Kuvshinov A, Langlais B, Léger JM, Lesur V, Livermore PW, Lowes FJ, Macmillan S, Magnes W, Mandea M, Marsal S, Matzka J, Metman MC, Minami T, Morschhauser A, Mound JE, Nair M, Nakano S, Olsen N, Pavón-Carrasco FJ, Petrov VG, Ropp G, Rother M, Sabaka TJ, Sanchez S, Saturnino D, Schnepf NR, Shen X, Stolle C, Tangborn A, Tøffner-Clausen L, Toh H, Torta JM, Varner J, Vervelidou F, Vigneron P, Wardinski I, Wicht J, Woods A, Yang Y, Zeren Z, Zhou B (2021) International geomagnetic reference field: the thirteenth generation. Earth, Planets and Space 73(1):49. https://doi.org/10.1186/s40623-020-01288-x

Aubert J (2023) State and evolution of the geodynamo from numerical models reaching the physical conditions of Earth's core. Geophys J Int 235(1):468–487. https://doi.org/10.1093/gji/ggad229

Ayala C, Beamud E, Huebert J, Jones SA, Kumar A, Miller SR, Moorkamp M, Pueyo EL, Ruiz-Constan A, Schamuells N, Sur D, Tauxe L, van Hinsbergen DJJ (2022) Geomagnetism, Paleomagnetism and Electromagnetism Perspectives on Integrated, Coordinated, Open, Networked (ICON) science. Earth and Space Science 9(6):e2021EA002141, https://doi.org/10.1029/2021EA002141

Barraclough DR (1987) International geomagnetic reference field: the fourth generation. Phys Earth Planet Inter 48(3):279–292. https://doi.org/10.1016/0031-9201(87)90150-6

Barraclough DR, Mundt W, Barker FS, Barton CE, Golovkov VP, Hood PJ, Lowes FJ, Peddie NW, Gui-zhong Q, Srivastava SP, Winch DE, Yukutake T, Zidarov DP, Chen-chang A, Estes RH, Kerridge DJ, Langel RA, Quinn JM, Sabaka TJ, Verhoef J (1987) International Geomagnetic Reference Field Revision 1987. J Geomagn Geoelectr 39(12):773–779. https://doi.org/10.5636/jgg.39.773

Barton CE (1997) International geomagnetic reference field: The seventh generation. J Geomagn Geoelectr 49(2–3):123–148. https://doi.org/10.5636/jgg.49.123

Beggan CD, Kloss A, Grayver A, Alken P, Balasis G, Brown W, Califf S, Chauvet L, Chulliat A, Fillion M, Gailler L, Hulot G, Korte M, Lesur V, Lin Y, Matsushima M, McCreadie H, Minami T, Nair M, Nakano S, Pàvon-Carrasco J, Rother M, Sato S, Serrano M, da Silva M, Smith A, Terra-Nova F, Thebault E, Toh H, Wardinski I, Xiong C (2026) Evaluation of candidate models for the 14th generation International Geomagnetic Reference Field. Earth Planets Space this issue. https://doi.org/10.1186/s40623-026-02382-2

Beggan CD (2022) Evidence-based uncertainty estimates for the International Geomagnetic Reference Field. Earth, Planets and Space 74(1):17. https://doi.org/10.1186/s40623-022-01572-y

Beggan C, Kloss C, Smith A, Amblard PO, Amezza T, Aubert J, Baerenzung J, Brown W, Califf S, Campuano S, Chulliat A, Claveau R, Davies C, Dobrovolsky M, Finlay C, Firsov I, Fournier A, Gailler L, Gillet N, Gomez Perez N, Grayver A, Gwirtz K, Hamoudi M, Holme R, Holschneider M, Jiang Y, Kada M, Korte M, Krasnoperov R, Kuang W, Kudin D, Lauridsen JB, Lemgharbi A, Lesur V, Liu P, Livermore P, Madsen F, Matsushima M, Matzka J, Michaelis I, Minami T, Nair M, Nakano S, Oehler JF, Olsen N, Pavón-Carrasco F, Presnyakov S, Qian B, Rang X, Rogers H, Rother M, Rouxel D, Sabaka T, Sato S, Saynisch-Wagner J, Schanner M, Serrano M, Shakespeare-Rees N, da Silva MV, Soloviev A, Thébault E, Tøffner-Clausen L, Toh H, Wang J, Wardinski I, Watson C, Whaler K, Xiong C, Yan Q, Yang Y, Yao H, Zeren Z, Zhang K, Zhou B (2024) IGRF-14 Evaluation. https://doi.org/10.5281/zenodo.14205635

Cain JC, Cain SJ (1971) Derivation of the International Geomagnetic Reference Field IGRF(10/68). Tech Rep. D-6237, NASA

Colomb F, Alonso C, Hofmann C, Nollmann I (2004) SAC-C mission, an example of international cooperation. Adv Space Res 34(10):2194–2199. https://doi.org/10.1016/j.asr.2003.10.039

Finlay CC, Maus S, Beggan CD, Bondar TN, Chambodut A, Chernova TA, Chulliat A, Golovkov VP, Hamilton B, Hamoudi M, Holme R, Hulot G, Kuang W, Langlais B, Lesur V, Lowes FJ, Lühr H, Macmillan S, Mandea M, McLean S, Manoj C, Menvielle M, Michaelis I, Olsen N, Rauberg J, Rother M, Sabaka TJ, Tangborn A, Tøffner-Clausen L, Thébault E, Thomson AWP, Wardinski I, Wei Z, Zvereva TI (2010) International Geomagnetic Reference Field: the eleventh generation. Geophys J Int 183(3):1216–1230. https://doi.org/10.1111/j.1365-246X.2010.04804.x

Finlay CC, Maus S, Beggan CD, Hamoudi M, Lowes FJ, Olsen N, Thébault E (2010) Evaluation of candidate geomagnetic field models for IGRF-11. Earth, Planets and Space 62(10):8

Finlay CC, Kloss C, Olsen N, Hammer MD, Tøffner-Clausen L, Grayver A, Kuvshinov A (2020) The CHAOS-7 geomagnetic field model and observed changes in the South Atlantic Anomaly. Earth, Planets and Space. https://doi.org/10.1186/s40623-020-01252-9

Friis-Christensen E, Lühr H, Hulot G (2006) Swarm: a constellation to study the Earth's magnetic field. Earth, Planets and Space 58(4):351–358

Hulot G, Lhuillier F, Aubert J (2010) Earth's dynamo limit of predictability. Geophys Res Lett. https://doi.org/10.1029/2009GL041869

Hulot G, Vigneron P, Léger JM, Fratter I, Olsen N, Jager T, Bertrand F, Brocco L, Sirol O, Lalanne X, Boness A, Cattin V (2015) Swarm's absolute magnetometer experimental vector mode, an innovative capability for space magnetometry. Geophys Res Lett. https://doi.org/10.1002/2014GL062700

IAGA Division I Study Group (1975) International Geomagnetic Reference Field 1975. J Geomagn Geoelectr 27(5):437–439. https://doi.org/10.5636/jgg.27.437

International Association of Geomagnetism and Aeronomy (2024) IGRF-14 coefficients. https://doi.org/10.5281/zenodo.14218973, https://doi.org/10.5281/zenodo.14218973
Jiang Y, Finlay CC, Olsen N, Tøffner-Clausen L, Yan Q, Zhang K (2024) Macau Scientific Satellite-1 initial magnetic field model. Geophysical Research Letters 51(22):e2024GL112305, https://doi.org/10.1029/2024GL112305
Langel RA (1992) International Geomagnetic Reference Field: the Sixth Generation. J Geomagn Geoelectr 44(9):679–707. https://doi.org/10.5636/jgg.44.679
Langel RA, Barraclough DR, Kerridge DJ, Golovkov VP, Sabaka TJ, Estes RH (1988) Definitive IGRF Models for 1945, 1950, 1955, and 1960. J Geomagn Geoelectr 40(6):645–702. https://doi.org/10.5636/jgg.40.645
Laundal KM, Soler S, Smith A, Skeidsvoll AS, Billett D, PB2 (2024) IAGA-VMOD/ppigrf: 2.0.0. https://doi.org/10.5281/zenodo.14231854
Laundal KM, Richmond AD (2017) Magnetic coordinate systems. Space Sci Rev 206(1–4):27–59
Léger JM, Jager T, Bertrand F, Hulot G, Brocco L, Vigneron P, Lalanne X, Chulliat A, Fratter I (2015) In-flight performance of the Absolute Scalar Magnetometer vector mode on board the Swarm satellites. Earth Planets Space. https://doi.org/10.1186/s40623-015-0231-1
Lowes F (2000) An estimate of the errors of the IGRF/DGRF fields 1945–2000. Earth, Planets and Space 52(12):1207–1211
Macmillan S, Maus S (2005) International geomagnetic reference field—the tenth generation. Earth, Planets and Space 57(12):1135–1140. https://doi.org/10.1186/BF03351896
Macmillan S, Maus S, Bondar T, Chambodut A, Golovkov V, Holme R, Langlais B, Lesur V, Lowes F, Lühr H, Mai W, Mandea M, Olsen N, Rother M, Sabaka T, Thomson A, Wardinski I (2003) The 9th-Generation International Geomagnetic Reference Field. Geophys J Int 155(3):1051–1056. https://doi.org/10.1111/j.1365-246X.2003.02102.x
Macmillan S, Finlay CC (2011) The International Geomagnetic Reference Field. In: Mandea M, Korte M (eds) Geomagnetic Observations and Models, vol 5. Springer, pp 265–276
Mandea M, Macmillan S (2000) International geomagnetic reference field—the eighth generation. Earth, Planets and Space 52(12):1119–1124. https://doi.org/10.1186/BF03352342
Maus S (2007) CHAMP, Springer Science & Business Media, pp 59–61
Maus S, Macmillan S, Chernova T, Choi S, Dater D, Golovkov V, Lesur V, Lowes F, Lühr H, Mai W, McLean S, Olsen N, Rother M, Sabaka T, Thomson A, Zvereva T (2005) The 10th-Generation International Geomagnetic Reference Field. Geophys J Int 161(3):561–565. https://doi.org/10.1111/j.1365-246X.2005.02641.x
Olsen N (2007) Ørsted, Encyclopedia of geomagnetism and paleomagnetism. Springer Science & Business Media, pp 743–746
Olsen N, Albini G, Bouffard J, Parrinello T, Tøffner-Clausen L (2020) Magnetic observations from CryoSat-2: calibration and processing of satellite platform magnetometer data. Earth, Planets and Space 72(1):48. https://doi.org/10.1186/s40623-020-01171-9
Peddie NW (1982) International Geomagnetic Reference Field: the Third Generation. J Geomagn Geoelectr 34(6):309–326. https://doi.org/10.5636/jgg.34.309
Raphaldini B, Medeiros ES, Ciro D, Franco DR, Trindade RIF (2021) Geomagnetic reversals at the edge of regularity. Phys Rev Res 3:013158. https://doi.org/10.1103/PhysRevResearch.3.013158
Rother M, Korte M, Morschhauser A, Vervelidou F, Matzka J, Stolle C (2021) The Mag.num core field model as a parent for IGRF-13, and the recent evolution of the South Atlantic Anomaly. Earth, Planets and Space 73(1):50. https://doi.org/10.1186/s40623-020-01277-0
Shen X, Zhang X, Yuan S, Wang L, Cao J, Huang J, Zhu X, Piergiorgio P, Dai J (2018) The state-of-the-art of the China Seismo-Electromagnetic Satellite mission. SCIENCE CHINA Technol Sci 61(5):634–642
Thébault E, Finlay CC, Beggan CD, Alken P, Aubert J, Barrois O, Bertrand F, Bondar T, Boness A, Brocco L, Canet E, Chambodut A, Chulliat A, Coïsson P, Civet F, Du A, Fournier A, Fratter I, Gillet N, Hamilton B, Hamoudi M, Hulot G, Jager T, Korte M, Kuang W, Lalanne X, Langlais B, Léger JM, Lesur V, Lowes FJ, Macmillan S, Mandea M, Manoj C, Maus S, Olsen N, Petrov V, Ridley V, Rother M, Sabaka TJ, Saturnino D, Schachtschneider R, Sirol O, Tangborn A, Thomson A, Tøffner-Clausen L, Vigneron P, Wardinski I, Zvereva T (2015) International Geomagnetic Reference Field: the 12th generation. Earth, Planets and Space 67:79. https://doi.org/10.1186/s40623-015-0228-9
Winch DE, Ivers DJ, Turner JPR, Stening RJ (2005) Geomagnetism and Schmidt quasi-normalization. Geophys J Int 160(2):487–504. https://doi.org/10.1111/j.1365-246X.2004.02472.x
Zhang K (2023) A novel geomagnetic satellite constellation: science and applications. Earth and Planetary Physics 7(1):4–21. https://doi.org/10.26464/epp2023019
Zmuda AJ (1971b) World magnetic survey 1957-1969. IAGA Bulletin No 28
Zmuda AJ (1971) The International Geomagnetic Reference Field: introduction. Bull Int Assoc Geomag Aeronomy 28:148–152

Publisher's Note